SUPPLEMENTAL MATERIAL

Supplemental Methods

Methodological Considerations

In an effort to use a model that is relevant to clinical post-MI LV remodeling and dysfunction, we selected a 2-h coronary occlusion – a duration of ischemia that would be expected to result in near-transmural infarcts in the rat. The success of this strategy is confirmed by our pilot studies, in which infarct size (measured at 24 h of reperfusion) was ≈ 90% of the risk region, and by our morphometric analysis, which showed the scar to average ≈ 50% of the risk region in the two groups. We chose a transient coronary occlusion followed by reperfusion (as opposed to a permanent coronary occlusion) because, in current practice, most patients with acute MI are reperfused, either spontaneously or iatrogenically. A 30-d interval following acute MI was selected because, by this time, the acute inflammatory response in the rat has resolved and the formation of the scar is complete. [1, 2] The relevance of this model of post-MI LV remodeling and cardiac failure is demonstrated by the presence of the cardinal features associated with this syndrome, including LV dilation, wall thinning, dysfunction, and fibrosis.

Isolation and Culture of CPCs

CPCs were isolated from the ventricle of adult Fischer 344 rats.[3] Clonogenic cells obtained by cell sorting and single cell cloning were infected with a retrovirus carrying EGFP.[4] A single clonogenic c-kit^{pos} cell expressing EGFP was used to develop a c-kit^{pos}-EGFP^{pos} clone, which was used in these studies.

Surgical Procedures

The methods were similar to those described previously [3]. Briefly, female Fischer 344 rats (age, 3 months; weight, 174 ± 2 g), were anesthetized with ketamine (37 mg/kg) and xylazine (5 mg/kg), intubated, and ventilated with a rodent respirator (Harvard Apparatus). Anesthesia was maintained with 1% isoflurane inhalation and body temperature was kept at 37°C with a heating pad. After administration of antibiotics, the chest was opened and the heart exposed. All rats underwent a 2-h occlusion of the left anterior descending coronary artery followed by reperfusion (supplemental Fig. 25). Thirty days later, the animals were randomly allocated to a control or a treated group. They were reanesthetized, the chest was reopened, and a thin catheter (Intracath, 24G, Becton Dickinson) was advanced into the aortic root through the left carotid artery. The ascending aorta and the pulmonary artery were occluded with a snare for two 20-s intervals, 10 min apart, during which time rats received an infusion of CPCs (1×10^6 in 1 ml of normal saline) or vehicle into the aortic root.[3] Rats were euthanized 35 days later; 0.1% 5-bromo-2′-deoxyuridine (BrdU) was given in the drinking water for the last two weeks before euthanasia. A separate group of four rats not subjected to surgery was used as a normal control for cardiac function and pathology.

Echocardiographic and Hemodynamic Studies

Serial echocardiograms were obtained at baseline (3 days before coronary occlusion), 30 days after MI (before treatment), and 35 days after treatment using an HDI 5000 SonoCT ultrasound system (Philips Medical Systems, Bothell, WA) equipped with 15-7 MHz linear broadband and 12-5 MHz phased array transducers.[3] Before echocardiography, rats were lightly anesthetized with pentobarbital (25 mg/kg i.p.). The anterior chest was shaved and the animals were placed

in the left lateral decubitus position. A rectal temperature probe was inserted, and the body temperature was carefully maintained between 37.0°C and 37.5°C with a heating pad throughout the study. The parasternal long-axis, parasternal short-axis, and apical four-chamber views were used to obtain 2D, M-mode, and spectral Doppler images.[3, 5] Systolic and diastolic anatomic parameters were obtained from M-mode tracings at the midpapillary level**.**

The hemodynamic studies were performed 35 days after treatment, just before euthanasia. Rats were anesthetized with ketamine (37 mg/kg) and xylazine (5 mg/kg), intubated, and mechanically ventilated. Anesthesia was maintained with 1% isoflurane and the core temperature kept at 37.0°C with a heating pad throughout the study. A 2F microtip pressure-volume (PV) catheter (SPR-869, Millar Instruments) was inserted into the right carotid artery and advanced into the LV cavity. The right jugular vein was cannulated for fluid administration. After 20 min of stabilization, the PV signals were recorded continuously with an ARIA PV conductance system (Millar Instruments) coupled with a Powerlab/4SP A/D converter (AD Instruments), stored, and displayed on a personal computer. PV relations were assessed by transiently compressing the inferior vena cava with a cotton swab [6]. Parallel conductance from surrounding structures was calculated by injecting a small bolus of 15% NaCl through the jugular vein.[6] Hemodynamic indexes were calculated using the PVAN 3.2 software (Millar Instruments).

Morphology and Histology

After the hemodynamic measurements, a polyethylene catheter filled with phosphate buffer (0.2 M, pH 7.4) and heparin (100 IU/ml) was advanced to the ascending aorta via the right carotid artery. In rapid succession, the heart was arrested in diastole by injecting 1.0 ml of a mixture of

cadmium chloride (100 mM)/potassium chloride (3 M) through the aortic catheter. The heart was then excised and perfused retrogradely with phosphate buffer for ~3 min to flush out residual blood in the coronary circulation, followed by perfusion with 10% neutral buffered formalin solution for 15 min. Perfusion pressure was maintained between 60 and 80 mmHg while end-diastolic pressure was kept at 8 mmHg. After perfusion-fixation, the atria and right ventricle were dissected from the LV. The LV weight and the longitudinal intracavitary axis (LV cavity length) were measured; LV volume was calculated as the difference between weight of the water-filled and empty LV by using the conversion of weight to volume (1 g H_2O = 1 ml H_2O).

The heart was cut into four transverse slices (~ 2-mm thick), which were processed, embedded in paraffin, sectioned at 4-μm intervals, and stained with Masson's trichrome, picrosirius red, or antibodies against EGFP and cell-type specific markers. Images were acquired digitally and analyzed using NIH ImageJ (1.37v). From the Masson's trichrome-stained images, morphometric parameters including LV cavity area, total LV area, risk region area, scar area, and LV wall thickness in the risk and noninfarcted regions were measured in each section (supplemental Fig. 10).[3] To quantitate both the degree of LV dilation and the degree of infarct wall thinning, the LV expansion index was calculated using a modification of the method of Hochman and Choo[7]: Expansion index = (LV cavity area/total area) x (noninfarcted region wall thickness/risk region wall thickness). Myocardial collagen content was quantitated on the picrosirius red-stained sections by determining collagen density (as percent area) under polarized light.[8]

To assess LV hypertrophy, in each heart the cross-sectional myocyte area was measured in 1-3 LV sections stained with WGA (supplemental Fig. 12A). At least 100 myocytes were measured in each heart (the total number of myocytes measured in each group is specified in supplemental Fig. 12). To evaluate cardiac fibrosis, LV sections were stained with picrosirius red (Fig. 4A) and collagen content was quantitated in images taken under polarized light (Fig. 4B).

To track the fate of transplanted CPCs, EGFP was detected in LV sections by immunofluorescence and analyzed by confocal microscopy.

Immunohistochemistry

Immunohistochemistry was performed in formalin-fixed, 4-μm-thick histological sections. All of the primary and secondary antibodies used in these studies are specified in supplemental Table 5. Persistence of transplanted CPCs (or their progeny) was detected with antibodies against EGFP. The fate of transplanted CPCs was assessed using the cell-type specific markers α-sarcomeric actin, α-actinin, myosin heavy chain (MHC), troponin I (TnI), α-smooth muscle actin (α-SMA), von Willebrand factor (vWF), and platelet-endothelial cell adhesion molecule (PECAM/CD31). Specifically, to determine whether, in the seven hearts in which $EGFP^{pos}$ cells were present, the transplanted CPCs differentiated toward a cardiac myogenic and/or vascular lineage, LV sections were stained for α-sarcomeric actin, MHC, α-actinin, TnI, α-SMA, vWF, and PECAM. Colocalization of these markers with EGFP was determined by confocal microscopy. Endogenous cardiac committed CPCs were identified as $c\text{-}kit^{pos}/EGFP^{neg}$ and counted by staining for the cardiac transcription factor Nkx2.5 and sarcomeric protein MHC in serial

sections (6 – 60x fields were counted in each of the risk and remote regions in one slice per heart). The number of endogenous CPCs (c-kit^{pos}/EGFP^{neg}) committed to the cardiac lineage (MHC^{pos}/NKX2.5^{pos}) was determined by staining one section for c-kit/EGFP/Nkx2.5/DAPI and the adjacent section for c-kit/EGFP/MHC/DAPI. Endogenous CPCs (c-kit^{pos}/EGFP^{neg}) were counted if they were clearly identified in both of the serial sections and scored for the presence or absence of MHC and Nkx2.5. Proliferation was assessed by immunofluorescent staining of nuclei for BrdU and Ki67. Myocyte cross-sectional area was determined by planimetry after staining cell membranes with FITC-conjugated wheat germ agglutinin (WGA). Cells undergoing apoptosis were detected by TUNEL staining.[9] Capillary density was assessed by staining tissue with FITC-conjugated isolectin B4.[10]

Real time PCR detection of the EGFP gene in transplanted CPC genomic DNA

As an alternative method of assessing engraftment of transplanted CPCs, real time PCR was used to detect the EGFP cDNA in hearts that received EGFP-labeled CPCs. DNA was isolated from a 180-µm thick section of a paraffin-embedded heart slice that had been used for immunohistochemical analysis. EGFP was amplified using Lux primers (Invitrogen); forward FAM labeled, cgggtGACGGCAACTACAAGACCcG, reverse, CTTCAGCTCGATGCGGTTCAC. EGFP was measured in each sample in two separate runs using 300 ng of input DNA using the Applied Biosystems 7900HT thermocycler with standard PCR cycling; 95C 15 s, 60C 60 s. DNA from EGFP expressing CPCs was used as positive control and to establish a standard curve to estimate the number of diploid copies per amount of input genomic DNA.

Statistical Analysis

Summary statistics are expressed as means ± SEM (standard error) or median (interquartile range). Data were analyzed using the Wilcoxon signed test or the Mann-Whitney Rank Sum Test for unpaired or paired experiments, as appropriate. Kruskal-Wallis one-way ANOVA on Ranks or Friedman's RM two-way ANOVA followed by Dunn's test was used for multiple group comparisons, as appropriate. Analyses were conducted with SigmaStat3.5. Values of $P<0.05$ were considered significant.

Supplemental Results

Pilot Studies

Pilot studies were performed to determine whether, in this strain of rats, a 2-h coronary occlusion would cause large infarcts (infarcts likely to result in LV remodeling). As illustrated in supplemental Fig. 26, after a 2-h occlusion/24-h reperfusion sequence, the extent of cell death (as assessed by tetrazolium staining) was nearly transmural and involved >90% of the risk region, indicating that this protocol does produce large infarctions.

Exclusions

Of the 46 rats operated upon, 11 died during the experiment (six of ventricular fibrillation during the 2-h coronary occlusion, one at 14 days after occlusion, and four during intracoronary infusion). Three rats were excluded because of extremely small infarcts (<10% of LV weight) (two in the vehicle and one in the CPC-treated group). Thus, a total of 32 rats (15 in the vehicle and 17 in the CPC-treated group) completed the protocol and were included in the final analysis. Furthermore, one rat (vehicle group) was excluded from the echocardiographic analysis because of inadequate images, two rats (CPC-treated group) were excluded from the hemodynamic

analysis because of technical failure during catheterization, and two rats (one in each group) were excluded from the morphometric analysis because of technical problems during the processing of the heart. Thus, the number of vehicle-treated and CPC-treated rats included in the final analysis was 14 and 17, respectively, for the echocardiographic data, 15 and 15 for the hemodynamic data, and 14 and 16 for the morphometric data.

Detection of Transplanted CPCs and Their Progeny

Surprisingly, despite careful analysis of four LV slices per heart, performed on 7-10 histologic sections in each slice at 40-80 μm intervals, $EGFP^{pos}$ cells were found in only seven of the 17 CPC-treated rats. In these seven hearts, $EGFP^{pos}$ cells were relatively rare, accounting for only 2.6 ± 1.1% of the area of the risk region and 1.1 ± 0.4% of the noninfarcted region (Fig. 5). These areas of EGFP positivity were calculated to correspond to 0.51 ± 0.21 x 10^6 $EGFP^{pos}$ cells/heart in the risk region and 1.05 ± 0.43 x 10^6 $EGFP^{pos}$ cells/heart in the noninfarcted region (Fig. 5B). (The lower number of $EGFP^{pos}$ cells despite the higher percent EGFP positivity in the risk region reflects the lower total number of cells in this region.) Thus, at 35 days after intracoronary infusion of CPCs, the transplanted cells (or their progeny) were present in a minority of the hearts and, in those, they occupied a small fraction of the myocardium.

EGFP real time PCR analysis

To verify the absence of EGFP labeled CPCs (or their progeny) in the subset of CPC-treated hearts that did not express EGFP ($EGFP^{neg}$ hearts), real time PCR was used to detect the EGFP cDNA that is present in the transplanted CPC genomic DNA. Of the 17 CPC-treated rats, 10 did not exhibit any $EGFP^{pos}$ cells by immunohistochemistry; in seven of these 10 $EGFP^{neg}$ hearts,

EGFP cDNA was not detected in genomic DNA isolated from paraffin embedded slices (supplemental Fig. 13A). Low EGFP copy numbers (3.5 to 15 per 300 ng genomic DNA, based on EGFP labeled CPC genomic DNA used as standard [supplemental Fig. 13B]) were found in the other three $EGFP^{neg}$ hearts and in one heart in the vehicle-treated group (supplemental Fig. 13A); these levels of cDNA are calculated to correspond to 9 to 38 cells per LV section. One limitation of this analysis is that precaution was not taken to prevent genomic DNA cross contamination of vehicle-treated hearts with material from CPC-treated hearts; thus, although every effort was made to avoid DNA cross contamination when isolating tissue from paraffin embedded heart slices to isolate genomic DNA, there may have been cross contamination prior to this step, i.e., during isolation of tissue. Accordingly, a false positive detection of EGFP cDNA may have occurred in the $EGFP^{neg}$ hearts, due to cross contamination.

Relationship Between Salubrious Effects of CPC Infusion and Presence of Transplanted CPCs at 35 Days

To elucidate whether the improved LV performance in the CPC-treated group was dependent on the presence of $EGFP^{pos}$ cells at 35 days, we examined separately the seven CPC-treated hearts that exhibited $EGFP^{pos}$ cells and the 10 hearts that displayed no EGFP positivity (supplemental Fig. 19). Morphometric analysis showed that the amount of viable myocardium in the risk region was significantly increased in both subsets relative to vehicle-treated hearts (supplemental Fig. 19A). The thickness of the anterior (infarcted) LV wall was significantly increased only in the $EGFP^{neg}$ hearts, and the LV expansion index was similar between the two subgroups. Echocardiographic (supplemental Fig. 19B) and hemodynamic (supplemental Fig. 19C) analysis revealed no consistent pattern favoring one subgroup over the other; both

EGFP^{pos} and EGFP^{neg} hearts exhibited evidence of functional improvement, although some functional parameters were improved in only one of these two subgroups. For example, echocardiographically measured LVEF was significantly increased in EGFP^{neg} but not EGFP^{pos} hearts (supplemental Fig. 19B), whereas the opposite was noted with hemodynamically measured LVEF (supplemental Fig. 19C); E_{es} was augmented in both subsets (supplemental Fig. 19C). Despite the obvious limitations of *a posteriori* subset analyses, these data suggest that the beneficial effects of exogenous CPCs do not depend on the presence of these cells, or their progeny, at 35 days after infusion.

To determine whether the EGFP^{pos} cell population proliferated at late (3-5 weeks) after transplantation, rats were given BrdU in the last 2 weeks of life and LV sections were stained with antibodies against BrdU and Ki67 (Figs. 7A and supplemental Fig. 20A).

SUPPLEMENTAL REFERENCES

1. Fishbein MC, Maclean D, Maroko PR. The histopathologic evolution of myocardial infarction. *Chest.* 1978;73(6):843-849.

2. Fishbein MC, Maclean D, Maroko PR. Experimental myocardial infarction in the rat: qualitative and quantitative changes during pathologic evolution. *Am J Pathol.* 1978;90(1):57-70.

3. Dawn B, Stein AB, Urbanek K, Rota M, Whang B, Rastaldo R, Torella D, Tang XL, Rezazadeh A, Kajstura J, Leri A, Hunt G, Varma J, Prabhu SD, Anversa P, Bolli R. Cardiac stem cells delivered intravascularly traverse the vessel barrier, regenerate

infarcted myocardium, and improve cardiac function. *Proc Natl Acad Sci U S A.* 2005;102(10):3766-3771.

4. Beltrami AP, Barlucchi L, Torella D, Baker M, Limana F, Chimenti S, Kasahara H, Rota M, Musso E, Urbanek K, Leri A, Kajstura J, Nadal-Ginard B, Anversa P. Adult cardiac stem cells are multipotent and support myocardial regeneration. *Cell.* 2003;114(6):763-776.

5. Stein AB, Tiwari S, Thomas P, Hunt G, Levent C, Stoddard MF, Tang XL, Bolli R, Dawn B. Effects of anesthesia on echocardiographic assessment of left ventricular structure and function in rats. *Basic Res Cardiol.* 2007;102(1):28-41.

6. Ito H, Takaki M, Yamaguchi H, Tachibana H, Suga H. Left ventricular volumetric conductance catheter for rats. *Am J Physiol.* 1996;270(4 Pt 2):H1509-1514.

7. Hochman JS, Choo H. Limitation of myocardial infarct expansion by reperfusion independent of myocardial salvage. *Circulation.* 1987;75(1):299-306.

8. Junqueira LC, Bignolas G, Brentani RR. Picrosirius staining plus polarization microscopy, a specific method for collagen detection in tissue sections. *Histochem J.* 1979;11(4):447-455.

9. Ding B, Price RL, Goldsmith EC, Borg TK, Yan X, Douglas PS, Weinberg EO, Bartunek J, Thielen T, Didenko VV, Lorell BH. Left ventricular hypertrophy in ascending aortic stenosis mice: anoikis and the progression to early failure. *Circulation.* 2000;101(24):2854-2862.

10. Tongers J, Knapp JM, Korf M, Kempf T, Limbourg A, Limbourg FP, Li Z, Fraccarollo D, Bauersachs J, Han X, Drexler H, Fiedler B, Wollert KC. Haeme oxygenase promotes progenitor cell mobilization, neovascularization, and functional recovery after critical hindlimb ischaemia in mice. *Cardiovasc Res.* 2008;78(2):294-300.

Supplemental Tables

Supplemental Table 2. Echocardiographic data

	Vehicle (n=14)	CPC-treated (n=16)
Baseline (before MI)		
IVSd (mm)	1.48 ± 0.14	1.36 ± 0.05
IVSs (mm)	2.58 ± 0.07	2.60 ± 0.09
LVEDD (mm)	5.48 ± 0.19	5.40 ± 0.14
LVESD (mm)	2.53 ± 0.21	2.50 ± 0.13
LVAd (mm^2)	22.41 ± 0.81	21.37 ± 0.80
LVAs (mm^2)	9.56 ± 0.45	10.95 ± 1.23
FS (%)	54.3 ± 2.9	54.1 ± 1.7
FAC (%)	57.4 ± 1.2	58.1 ± 4.7
EF (%)	81.4 ± 2.3	81.7 ± 1.3
LVEDV (µl)	159.0 ± 8.3	159.5 ± 8.7
LVESV (µl)	52.8 ± 3.0	51.0 ± 2.1
IW ThF (%)	89.8 ± 6.1	91.9 ± 5.9
30 days after MI (before treatment)		
IVSd (mm)	1.03 ± 0.10	1.08 ± 0.08
IVSs (mm)	1.17 ± 0.09	1.22 ± 0.09
LVEDD (mm)	7.39 ± 0.14	7.29 ± 0.17
LVESD (mm)	5.95 ± 0.15	5.92 ± 0.21
LVAd (mm^2)	44.98 ± 1.63	44.65 ± 2.50
LVAs (mm^2)	31.91 ± 1.12	31.50 ± 1.79
FS (%)	19.4 ± 1.5	19.0 ± 1.6
FAC (%)	28.9 ± 1.4	29.3 ± 1.7
EF (%)	34.7 ± 2.4	33.9 ± 2.4
LVEDV (µl)	344.5 ± 13.7	359.6 ± 14.3
LVESV (µl)	238.2 ± 13.3	252.0 ± 13.6
IW ThF (%)	19.1 ± 6.3	13.9 ± 4.0
35 days after Treatment		
IVSd (mm)	0.72 ± 0.03^{a}	0.90 ± 0.06^{ab}
IVSs (mm)	0.88 ± 0.04^{a}	1.13 ± 0.06
LVEDD (mm)	8.08 ± 0.17^{a}	7.74 ± 0.21
LVESD (mm)	6.77 ± 0.17^{a}	6.21 ± 0.22
LVAd (mm^2)	49.74 ± 3.09	46.28 ± 2.75
LVAs (mm^2)	36.08 ± 2.65	33.68 ± 2.22
FS (%)	16.2 ± 1.1^{a}	20.0 ± 1.2^{b}
FAC (%)	28.1 ± 2.2	27.4 ± 1.8
EF (%)	29.6 ± 1.8^{a}	35.8 ± 1.9^{b}
LVEDV (µl)	371.1 ± 27.5	324.7 ± 18.1
LVESV (µl)	256.5 ± 25.0	217.8 ± 13.7
IW ThF (%)	17.1 ± 2.6	26.4 ± 3.4^{ab}

IVSd, interventricular septal thickness at diastole; **IVSs**, interventricular septal thickness at systole; **LVEDD,** left ventricular end-diastolic diameter; **LVESD**, left ventricular end-systolic diameter; **LVAd**, left ventricular area at diastole; **LVAs**, left ventricular area at systole; **FS**, fractional shortening; **FAC**, fractional area change; **EF**, ejection fraction; **LVEDV**, left ventricular end-diastolic volume; **LVESV**, left ventricular end-systolic volume; **IW ThF**; infarct wall thickening fraction. ***a***, $P<0.05$ vs. 30 days after MI, ***b***, $P<0.05$ vs. vehicle group.

Supplemental Table 3. Hemodynamic Variables

	(n=4)	Vehicle (n=15)	CPC-treated (n=15)
Heart rate (bpm)	365 ± 13	308 ± 10[a]	306 ± 13[a]
LV End-Diastolic Volume (µl)	238 ± 32	336 ± 22[a]	324 ± 22
LV End-Systolic Volume (µl)	80 ± 24	223 ± 13[a]	193 ± 14[a]
LV End-Systolic Pressure (mmHg)	136.9 ± 3.4	107.1 ± 5.3[a]	114.5 ± 4.1[a]
LV End-Diastolic Pressure (mmHg)	6.0 ± 0.8	11.5 ± 0.4[a]	9.4 ± 0.5[ac]
Stroke Volume (µl)	185.8 ± 16.1	132.0 ± 12.9	140.1± 13.3
Ejection Fraction (%)	79.9 ± 4.9	38.3 ± 2.1[a]	44.5 ± 2.2[ab]
dP/dt max (mmHg/sec)	8791 ± 107	5160 ± 392[a]	6471 ± 363[ab]
dP/dt min (mmHg/sec)	7844 ± 655	4181 ± 340[a]	4661 ± 307[a]
Cardiac Output (mL/min)	67704 ± 6015	41590 ± 5070[a]	43692 ± 4912[a]
Stroke Work (mmHg*µl)	20287 ± 2777	11610 ± 1413[a]	12907± 1632[a]
P@dPdt max (mmHg)	73.9 ± 3.4	59.3 ± 3.4[a]	63.8 ± 3.0
Tau_l (msec)	6.04 ± 0.25	8.68 ± 0.41[a]	8.03 ± 0.23[a]
Maximal Power (mWatts)	96.7 ± 10.5	45.9 ± 7.3[a]	52.1 ± 9.3[a]
Preload adjusted maximal power (mWatts/µl^2)	28.0 ± 10.0	4.0 ± 0.3[a]	5.5 ± 0.6[ab]
E*es*	2.76 ± 0.42	0.64 ± 0.08[a]	1.11 ± 0.12[ac]
PRSW	144.1 ± 18.5	69.7 ± 8.0[a]	92.5 ± 8.0[a]
slope-EDPVR	0.03 ± 0.01	0.04 ± 0.02	0.04 ± 0.02
E*max*	3.89 ± 0.36	1.06 ± 0.14[a]	1.67 ± 0.16[ac]
dP/dt - EDV	52.2 ± 3.6	29.5 ± 4.2[a]	41.9 ± 10.6
dP/dt *max*-EDV	39.6 ± 6.9	15.7 ± 1.3[a]	20.8 ± 1.3[ac]
dP/dt *max*-P-dP/dt	119.9 ± 6.7	85.6 ± 2.9[a]	101.6 ± 3.5[ac]

Tau_1, Tau-logistic method; **E*es***, end-systolic elastance; **PRSW**, pre-load recruitable stroke work; **EDPVR**, end-diastolic pressure-volume relationship; **E*max***, maximal elastance during a cardiac circle; **EDV**, end-diastolic volume. ***a***, P<0.05 vs. normal; ***b***, P<0.05, and ***c***, P<0.01 vs. vehicle.

Supplemental Table 4. Morphometric data

	Vehicle (n=14)	**CPC-treated (n=16)**
Epicardial area (mm^2)	53.2 ± 2.4	54.0 ± 2.1
Endocardial area (mm^2)	22.0 ± 1.6	19.3 ± 2.1
Risk region area (mm^2)	12.9 ± 0.90	14.4 ± 1.0
Scar area (mm^2)	7.2 ± 0.7	6.5 ± 0.6
Scar thickness (mm)	1.2 ± 0.1	1.5 ± 0.1[a]
Septum thickness (mm)	2.0 ± 0.1	2.2 ± 0.1
Total LV wall area (mm^2)	31.3 ± 1.7	34.7 ± 1.0
Risk (% of LV)	41.0 ± 1.7	41.8 ± 3.0
Scar (% of total LV wall)	22.7 ± 1.1	18.8 ± 1.9
Scar (% of risk region)	55.6 ± 2.2	44.4 ± 2.2[a]
Viable tissue (% of risk region)	44.4 ± 2.2	55.7 ± 2.2[a]
Infarct expansion index	1.15 ± 0.12	0.88 ± 0.05[a]

a , $P < 0.05$ vs. vehicle

Supplemental Table 5. Antibodies used for the studies

Antigen	Primary Antibody	Secondary Antibody	Procedure
Myosin heavy chain	Mouse Monoclonal (Abcam)	Cy5- or TRITC-conjugated donkey anti-mouse	IHC
Alpha actinin	Mouse Monoclonal (Sigma)	TRITC-conjugated donkey anti-mouse	IHC
Cardiac troponin-I	Goat Polyclonal (Santa Cruz)	TRITC-conjugated donkey anti-goat	IHC
Connexin43	Rabbit polyclonal (Sigma)	FITC-conjugated donkey anti-rabbit	IHC
N-Cadherin	Rabbit polyclonal (Santa Cruz)	FITC-conjugated donkey anti-rabbit	IHC
von Willebrand factor	Rabbit polyclonal (DAKO), Mouse Monoclonal (Serotec)	FITC-conjugated donkey anti-rabbit, FITC-conjugated donkey anti-mouse	IHC
PECAM/CD31	Rabbit Polyclonal (Santa Cruz)	FITC-conjugated donkey anti-rabbit	IHC
c-kit	Goat polyclonal (R&D), Rabbit Polyclonal (Santa Cruz)	FITC-conjugated donkey anti-goat, FITC-conjugated donkey anti-rabbit, and TRITC-conjugated donkey anti-rabbit	IHC
α–smooth muscle actin	Mouse Monoclonal (Sigma)	TRITC-conjugated donkey anti-mouse	IHC
α–sarcomeric actin	Mouse Monoclonal (Sigma)	TRITC-conjugated donkey anti-mouse, Cy5 conjugated donkey anti-mouse	IHC
BrdU	Mouse Monoclonal (Roche)	FITC-conjugated sheep anti-mouse	IHC
EGFP	Rabbit Polyclonal (Molecular Probes)	FITC-conjugated donkey anti-rabbit, TRITC conjugated donkey anti-rabbit	IHC
EGFP	Goat Polyclonal (Abcam)	FITC-conjugated donkey anti-goat, TRITC-conjugated donkey anti-goat	IHC
EGFP primary conjugated	Rabbit Polyclonal (Molecular Probes)Alex 488		IHC
Ki67	Rabbit Polyclonal (Vector)	FITC-conjugated donkey anti-rabbit	IHC
Nkx2.5	Goat Polyclonal (Santa Cruz)	TRITC-conjugated donkey anti-goat	NA
Isolectin B4	Vector Labs	NA	NA
WGA	Molecular Probes	NA	NA

IHC, immunohistochemistry.

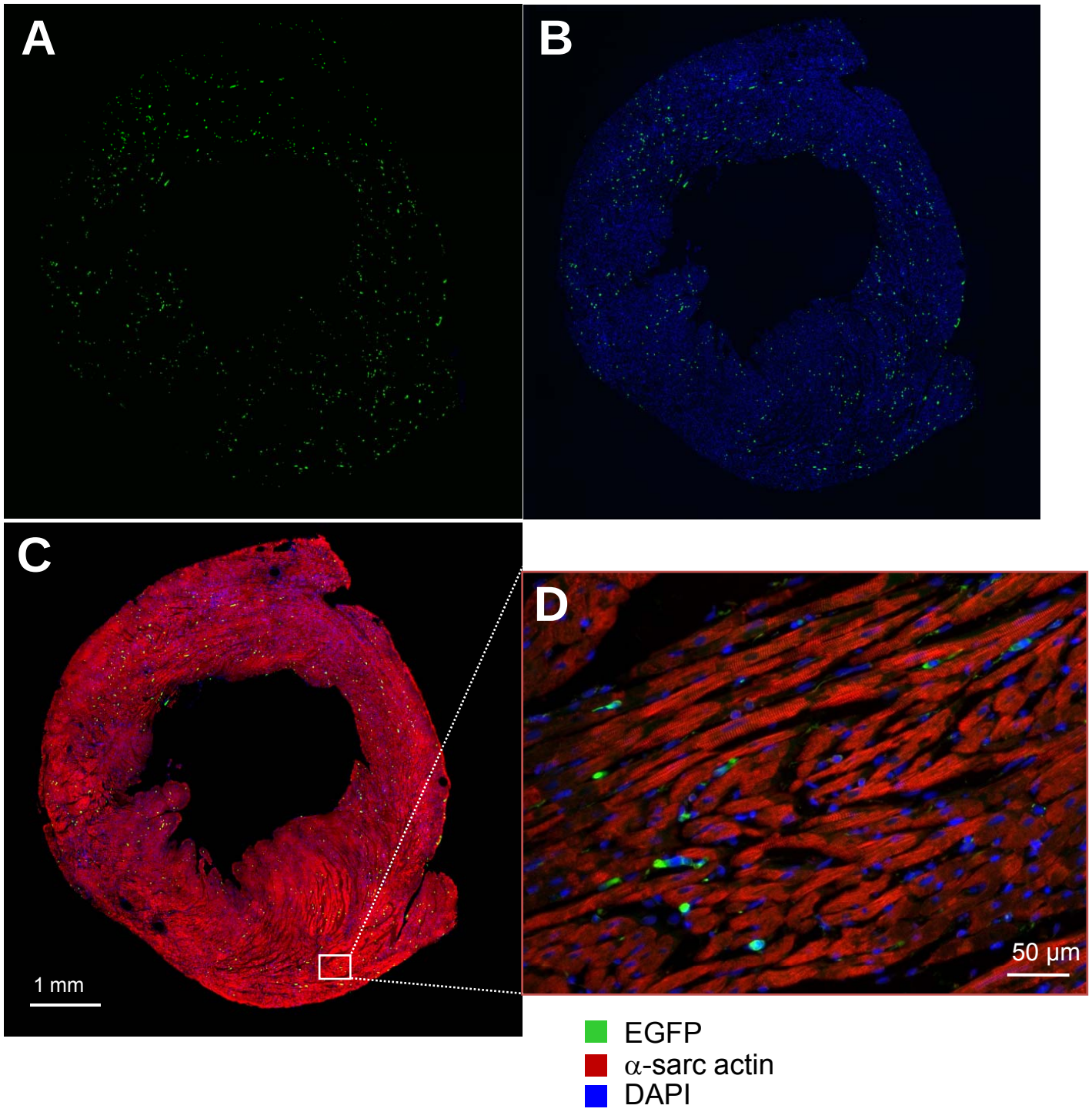

Supplemental Figure 9. **Distribution of EGFP-labeled CPCs in the heart following intracoronary infusion.** Microscopic images of an LV section from a normal rat that received EGFP-labeled CPCs as described in the text (two infusions via a catheter positioned in the aortic root during two episodes of 20-s occlusion of the ascending aorta and pulmonary artery, 10 min apart; total of $1x10^6$ cells in 1 ml) and was sacrificed 5 min after the second infusion. ***(A)*** Immunofluorescent staining for EGFP (green); ***(B)*** immunofluorescent staining for EGFP and staining for DAPI; ***(C)*** immunofluorescent staining for EGFP and α-sarcomeric actin (red) and staining for DAPI; ***(D)*** magnification of the box in ***C***. Note that numerous $EGFP^{pos}$ cells were distributed homogenously in the entire LV section. (The free right ventricular wall has been cut.)

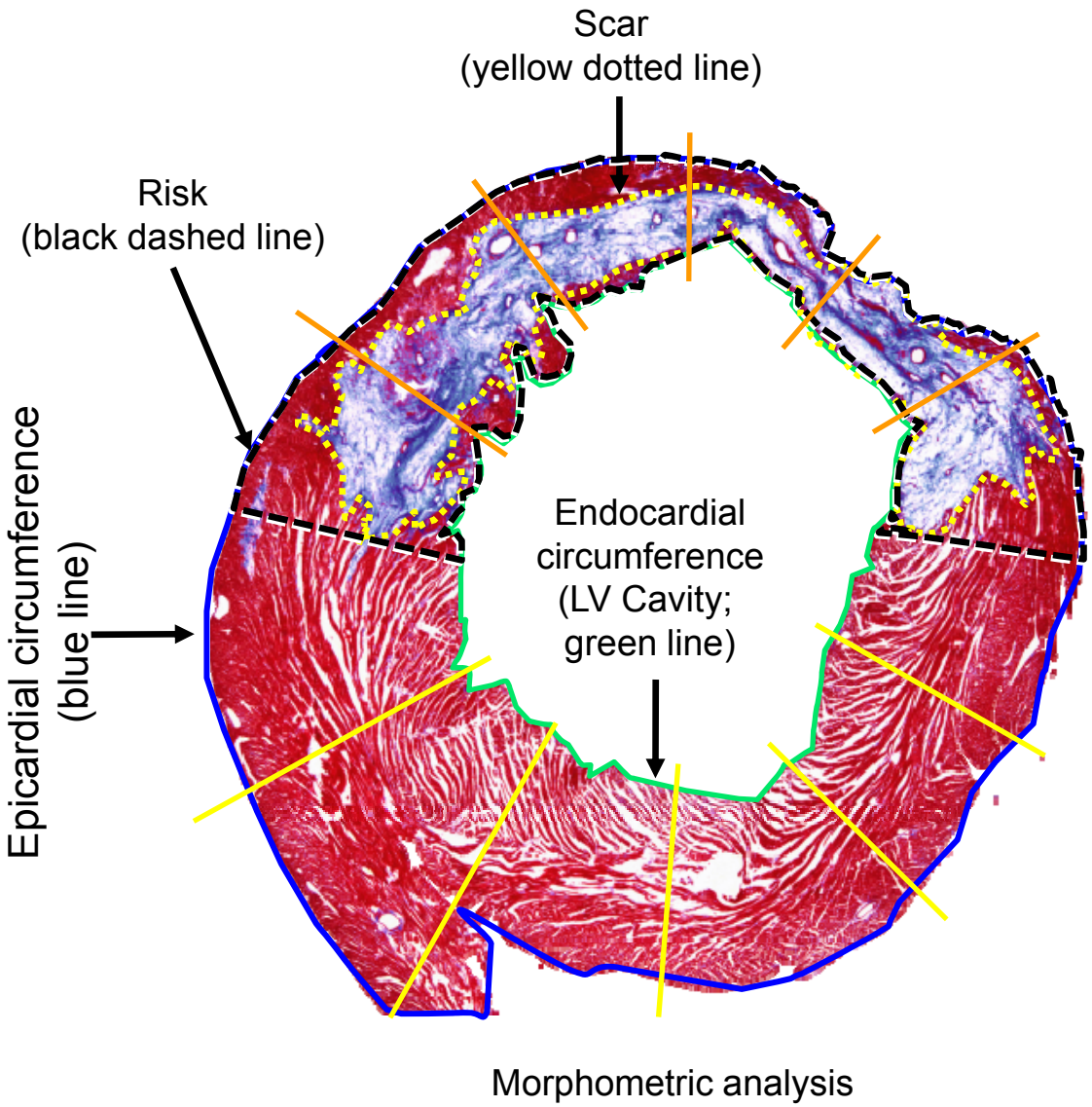

<u>Supplemental Figure 10</u>. Methods used to define and measure morphometric variables. The **risk region** was defined as the LV area between the two edges of the infarct scar ***(black dashed lines)***; **LV cavity**, the area within the endocardial circumference; **total LV area**, the area within the epicardial circumference; **scar region**, the area within the ***yellow dotted line***; **infarcted wall thickness,** average of 5 measurements of LV wall thickness equally distributed within the infarcted LV region as indicated by the ***orange lines***; **noninfarcted wall thickness,** average of 5 measurements equally distributed within the posterior wall as indicated by the ***yellow lines***. **LV expansion index** was calculated as the ratio of the endocardial circumference to the epicardial circumference divided by the ratio of posterior wall thickness to the anterior wall thickness ([endo circumference/epi circumference] / [posterior wall thickness/anterior wall thickness]).

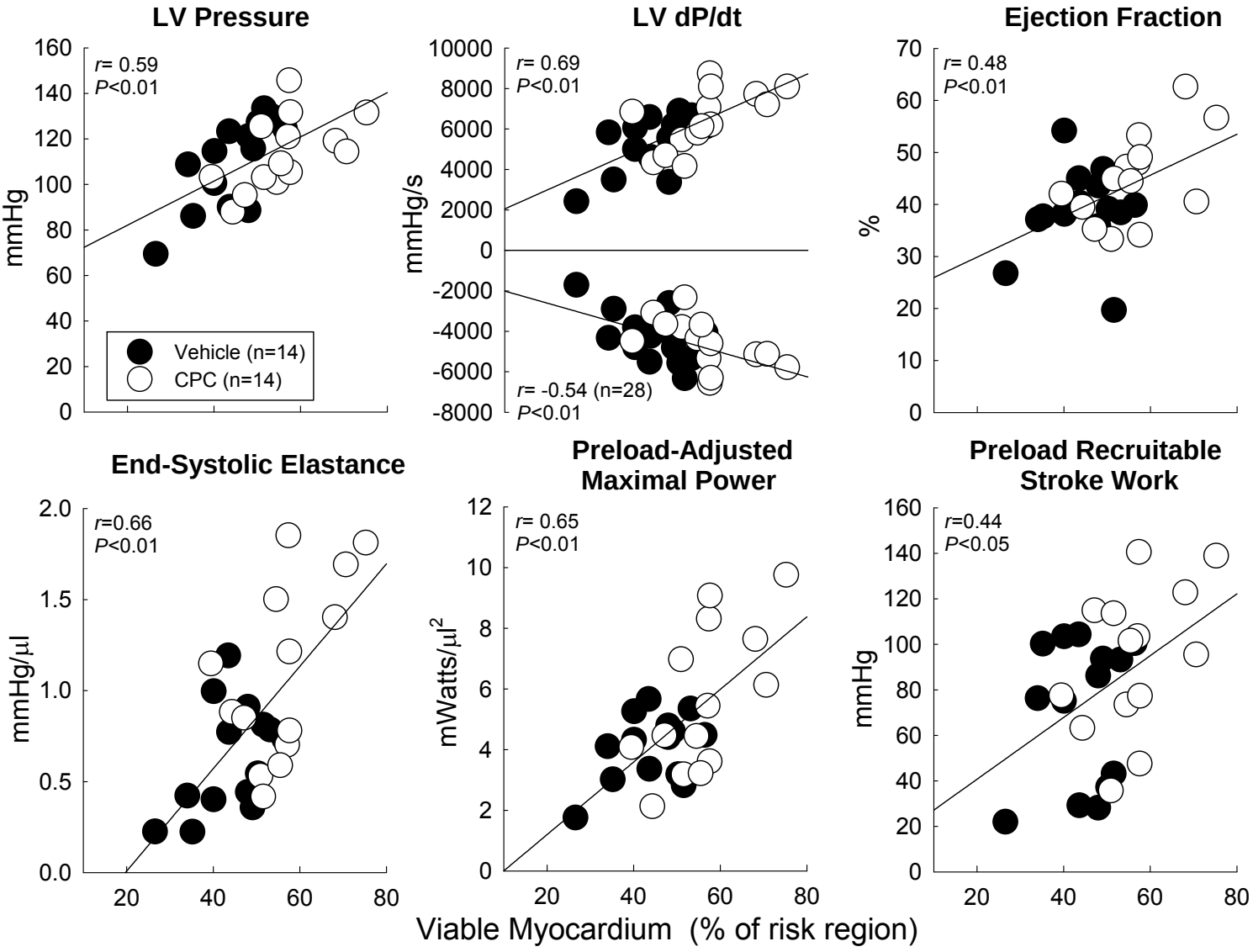

<u>Supplemental Figure 11</u>. Correlation between the amount of viable myocardium in the risk region and hemodynamic variables including LV pressure, dP/dt, ejection fraction, end-systolic elastance, preload-adjusted maximal power, and preload recruitable stroke work. Correlation analyses were performed by pooling all rats together, regardless of treatment, although the distribution is illustrated separately for vehicle-treated (solid circles) and CPC-treated rats (open circles).

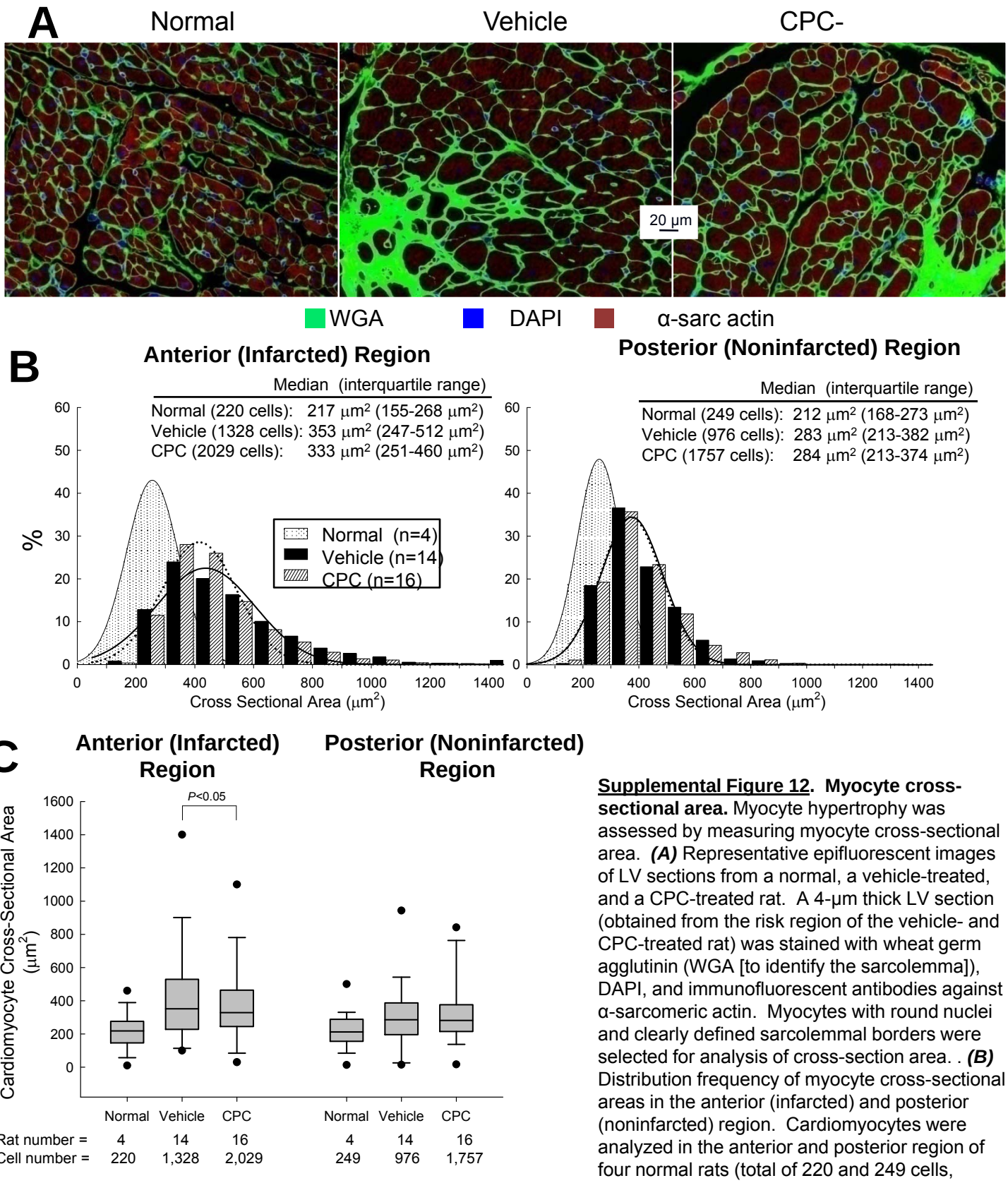

Supplemental Figure 12. Myocyte cross-sectional area. Myocyte hypertrophy was assessed by measuring myocyte cross-sectional area. ***(A)*** Representative epifluorescent images of LV sections from a normal, a vehicle-treated, and a CPC-treated rat. A 4-μm thick LV section (obtained from the risk region of the vehicle- and CPC-treated rat) was stained with wheat germ agglutinin (WGA [to identify the sarcolemma]), DAPI, and immunofluorescent antibodies against α-sarcomeric actin. Myocytes with round nuclei and clearly defined sarcolemmal borders were selected for analysis of cross-section area. . ***(B)*** Distribution frequency of myocyte cross-sectional areas in the anterior (infarcted) and posterior (noninfarcted) region. Cardiomyocytes were analyzed in the anterior and posterior region of four normal rats (total of 220 and 249 cells, respectively), 14 vehicle-treated rats (1,328 and 976 cells), and 16 CPC-treated rats (2,029 and 1,757 cells). In the anterior wall, the distribution was significantly different between vehicle- and CPC-treated rats ($P<0.05$). (**C**) Box-and-whisker plots showing **c**ardiomyocyte cross-sectional area in the anterior (infarcted) and posterior (noninfarcted) LV region of normal, vehicle-treated, and CPC-treated rats. Boxes show the median and the 1st and 3rd quartile (25th and 75th percentile); whiskers show the 1st and last decile (10th and 90th percentile); dots show the smallest and largest observations. Relative to normal rats, in both vehicle- and CPC-treated rats the distribution of myocyte cross-sectional areas was shifted to the right and the median area was increased, both in the risk region (anterior wall) (+~60%) and in the noninfarcted region (posterior wall) (+~30%). Although in the risk region the median myocyte cross-sectional area was slightly smaller ($P<0.05$) in the CPC-treated vs. the vehicle-treated group, no difference was observed in the noninfarcted region.

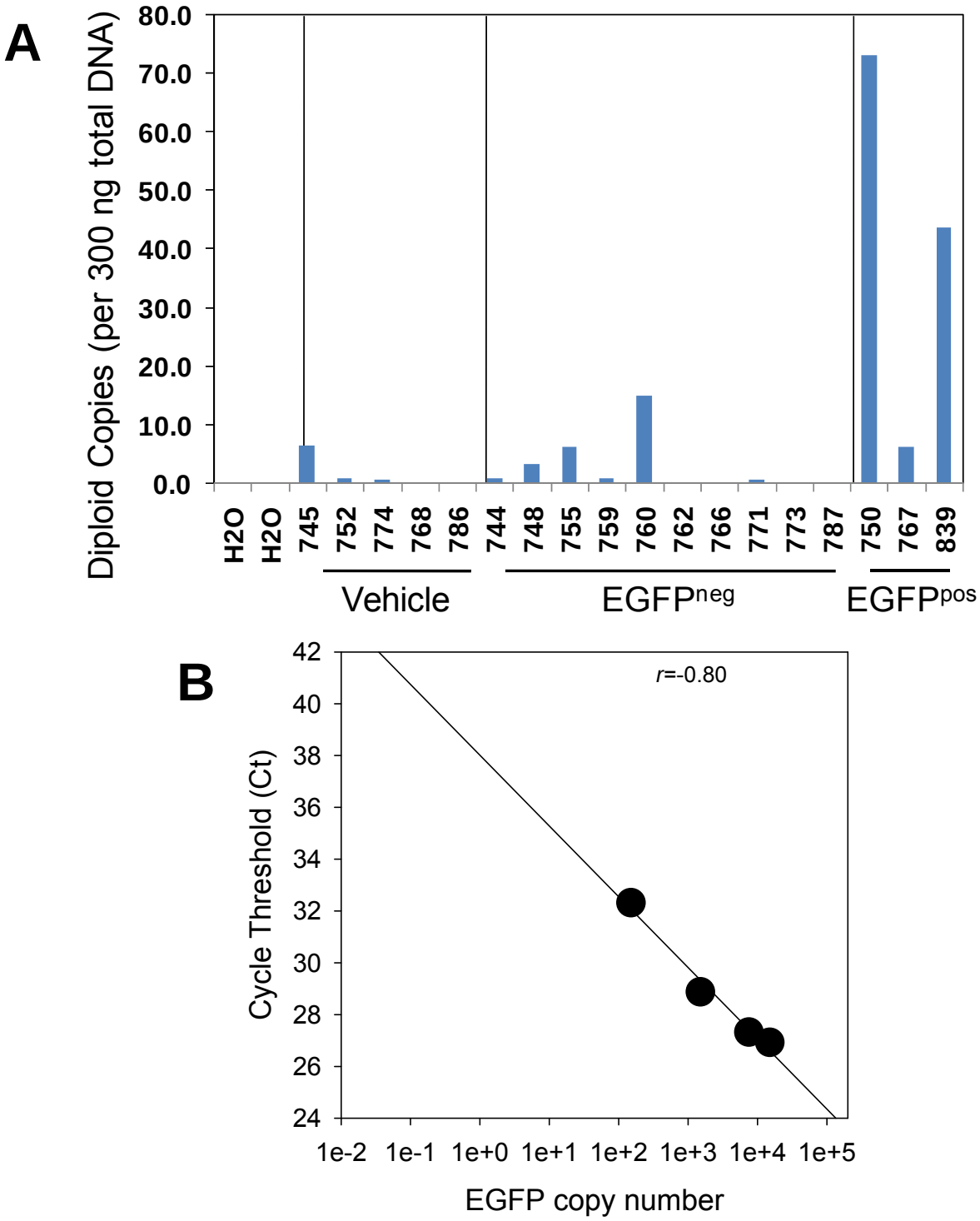

Supplemental Figure 13. EGFP real time PCR analysis. To verify the absence of EGFP^{pos} CPCs in CPC^{neg} treated hearts, the sensitive technique of real time PCR was used to detect the EGFP cDNA in genomic DNA isolated from the same samples used for immunohistochemical analysis. *(**A**)* In 300ng of DNA from each heart no signal was seen in 7 of the 10 EGFP^{neg} CPC treated hearts, confirming histological analysis. In 3 of the 10 EGFP^{neg} CPC treated hearts (748, 755, and 760), a small but reproducible signal was obtained (4-15 copies based on estimation from the standard curve in panel B) suggesting that in the 180 um tissue section used to obtain genomic DNA several copies of EGFP cDNA could be detected. Samples 750, 767 and 839 are EGFP^{pos} and were used as positive controls *(**B**)* Genomic DNA isolated from EGFP labeled CPCs used for transplantation was used to create a standard curve to estimate the copy number of EGFP cDNA detected in sample heart genomic DNA. The data are the mean of two experiments.

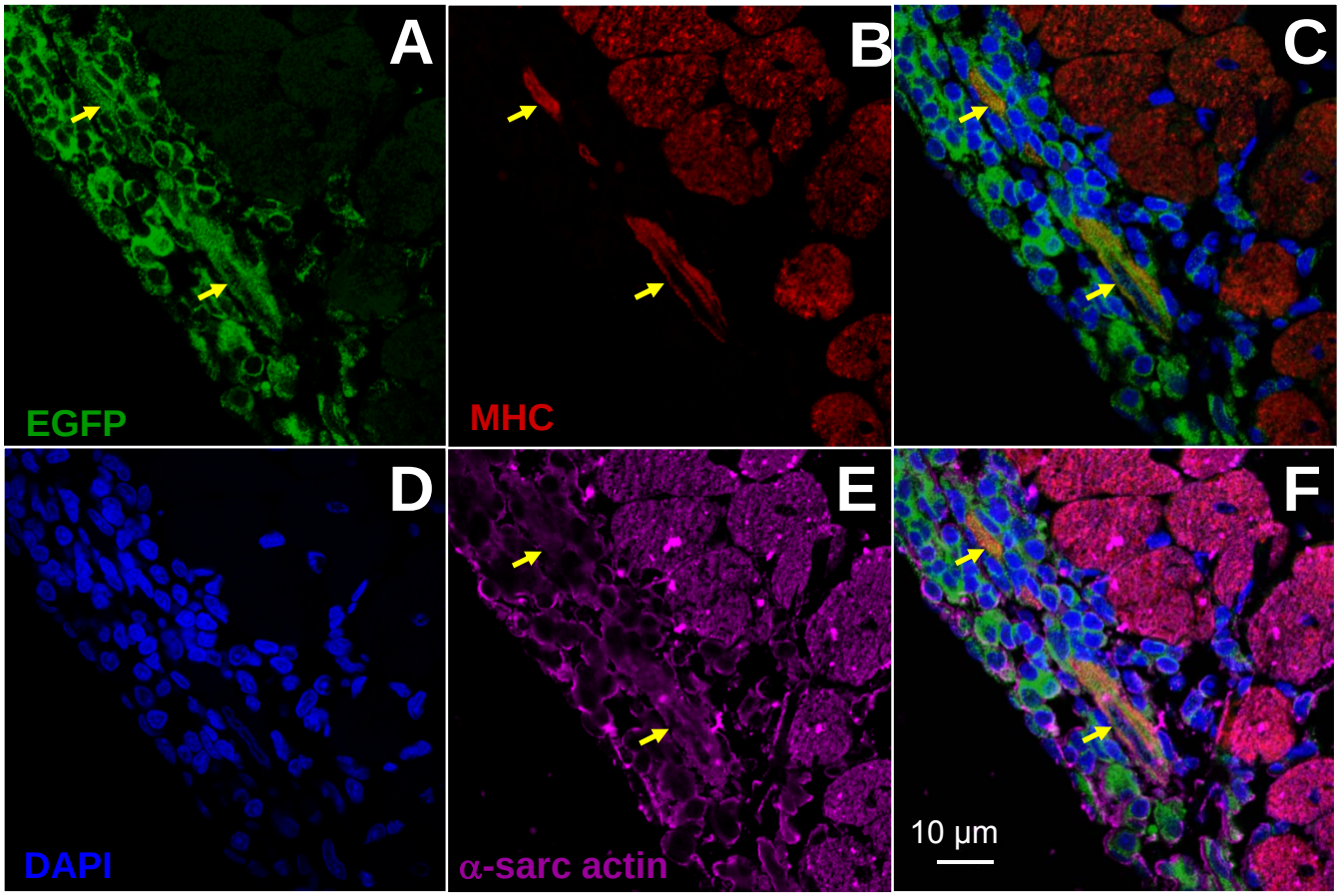

Supplemental Figure 14. **Expression of cardiac-specific proteins in EGFP^{pos} cells.** Representative confocal microscopic images showing colocalization of EGFP with myosin heavy chain (MHC) and α-sarcomeric actin in the border zone of a CPC-treated rat. ***(A)*** EGFP, ***(B)*** MHC, ***(E)*** α-sarcomeric actin, ***(D)*** DAPI, ***(C)*** merge of EGFP, MHC, and DAPI staining, ***(F)*** merge of EGFP, α-sarcomeric actin, and DAPI staining. **Yellow arrows** indicate EGFP^{pos} cells that express MHC and α-sarcomeric actin. Under epifluorescent microsopy, EGFP^{pos}/α-sarcomeric actin^{pos} cells (cells with colocalization of EGFP [FITC] and α-sarcomeric actin [TRITC]) were counted in the respective fluorescent emission channel. In each heart, one LV slice was selected for quantitation and 2-18 fields were counted (60x magnification; range, 53-387 cells per slice). Similar methods were used for other cardiac specific proteins.

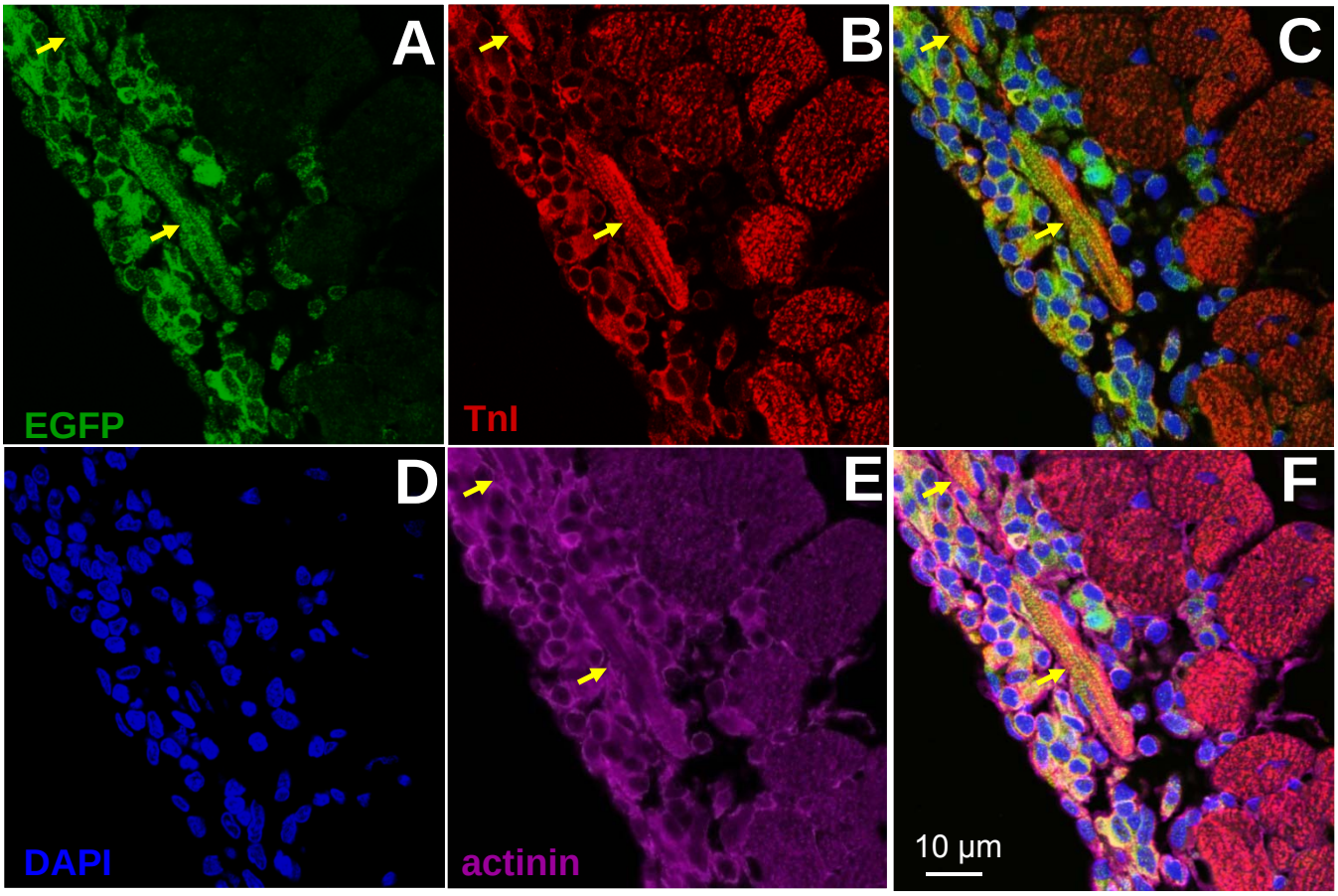

Supplemental Figure 15. Expression of cardiac-specific proteins in EGFP^{pos} cells. Representative confocal microscopic images (same LV section as the previous figure) showing colocalization of EGFP with troponin I (TnI) and actinin in the border zone of a CPC-treated rat. ***(A)*** EGFP, ***(B)*** TnI, ***(E)*** actinin, ***(D)*** DAPI, ***(C)*** merge of EGFP, TnI, and DAPI staining, ***(F)*** merge of EGFP, actinin, and DAPI staining. **Yellow arrows** indicate EGFP^{pos} cells that express TnI and actinin. Note that the cells indicated by yellow arrows express four cardiac-specific proteins (MHC, α-sarcomeric actin, TnI, and actinin).

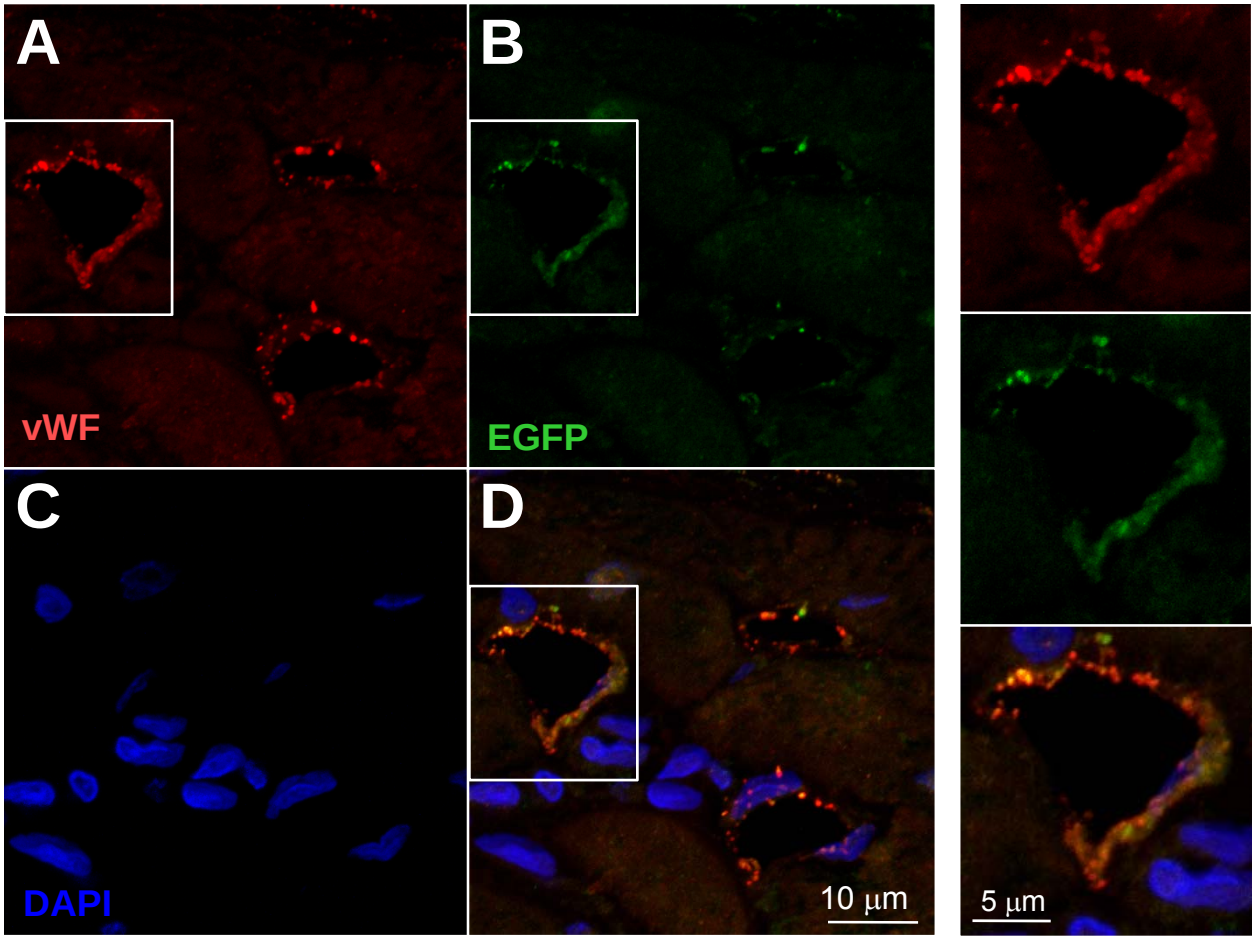

Supplemental Figure 16. **Expression of endothelial proteins (von Willebrand factor) in EGFP^{pos} cells.** Representative confocal microscopic images showing colocalization of EGFP with von Willebrand factor (vWF) in an arteriole in the border zone of a CPC-treated rat. ***(A)*** vWF, ***(B)*** EGFP, ***(C)*** DAPI, ***(D)*** merge of vWF, EGFP, and DAPI staining (the white box is magnified in the three panels on the right). The colocalization of EGFP with vWF suggests that transplanted CPCs participated in regeneration of vascular structures, differentiating into endothelial cells.

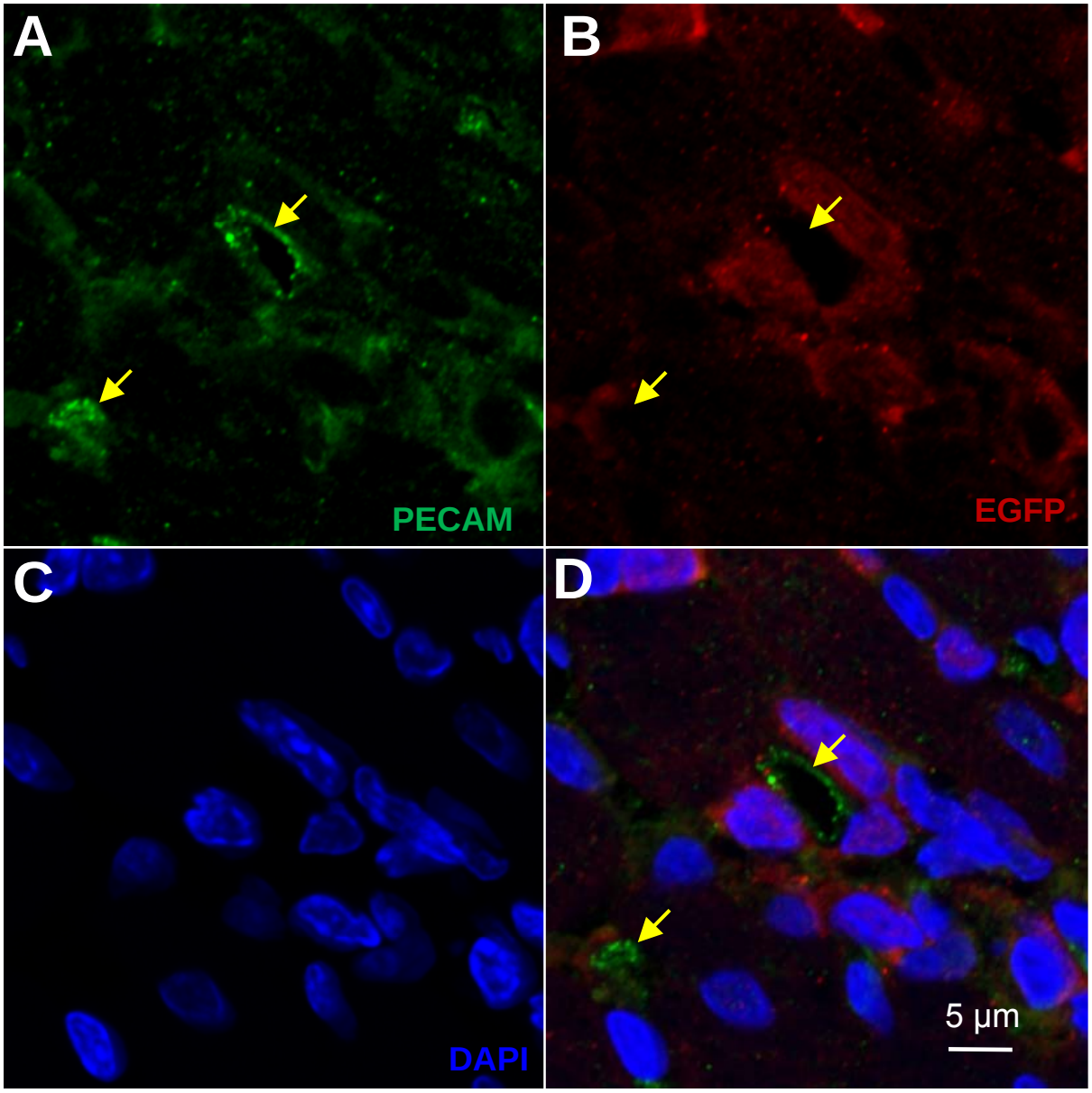

Supplemental Figure 17. **Expression of endothelial proteins (PECAM) in EGFP^{pos} cells.** Representative confocal microscopic images showing colocalization of EGFP with PECAM in the border zone of a CPC-treated rat. PECAM, platelet-endothelial cell adhesion molecule. ***(A)*** PECAM, ***(B)*** EGFP, ***(C)*** DAPI, ***(D)*** merge of PECAM, EGFP, and DAPI staining. The colocalization of EGFP with PECAM suggests that transplanted CPCs participated in regeneration of vascular structures, differentiating into endothelial cells.

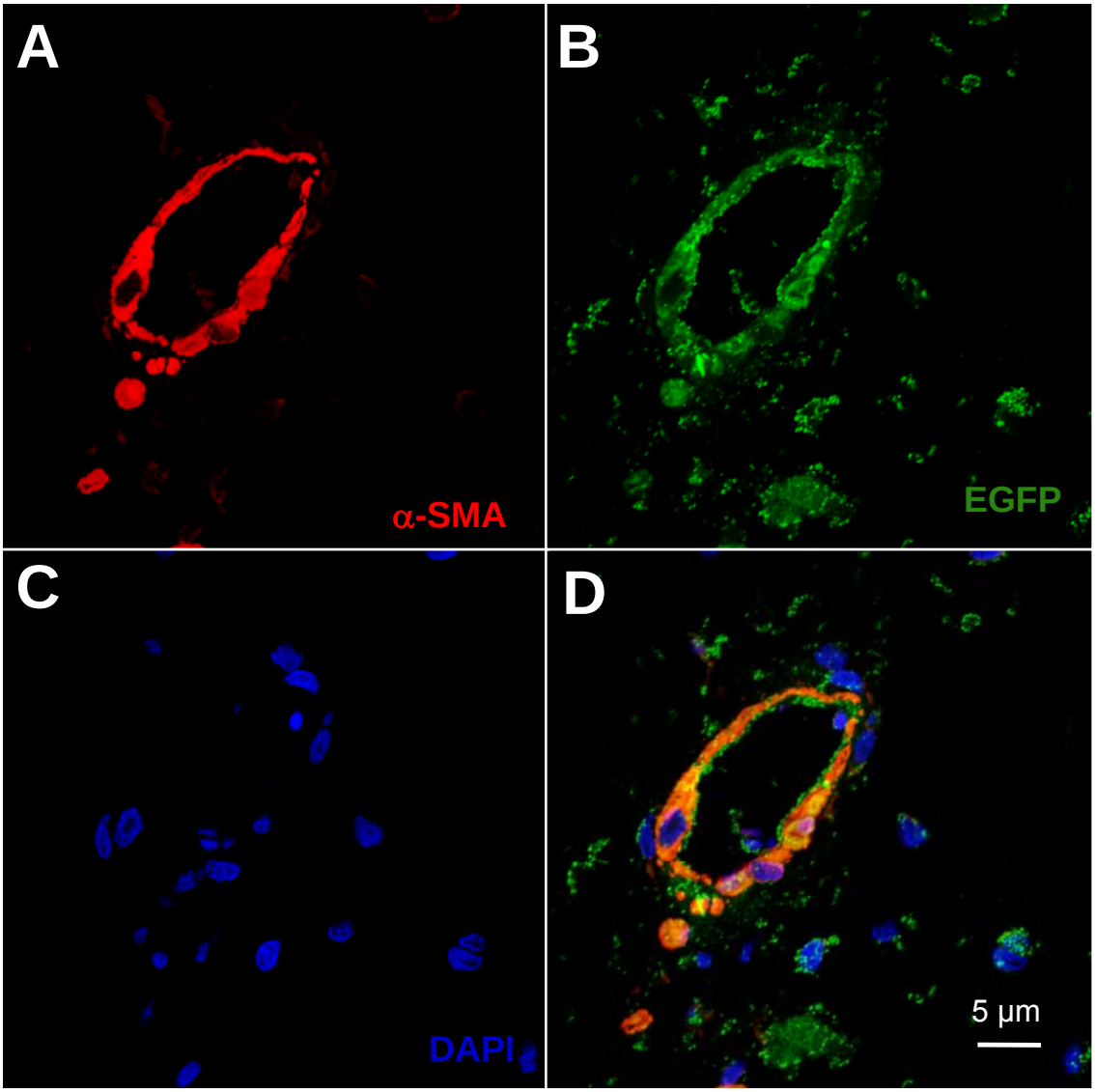

Supplemental Figure 18. **Expression of vascular smooth muscle proteins (α-smooth muscle actin) in EGFP^{pos} cells.** Representative confocal microscopic images showing colocalization of EGFP with α-smooth muscle actin (α-SMA) in the border zone of a CPC-treated rat. ***(A)*** α-SMA, ***(B)*** EGFP, ***(C)*** DAPI, ***(D)*** merge of α-SMA, EGFP, and DAPI staining. The colocalization of EGFP with α-SMA suggests that transplanted CPCs participated in regeneration of vascular structures, differentiating into smooth muscle cells. The structures illustrated here are most likely arterioles.

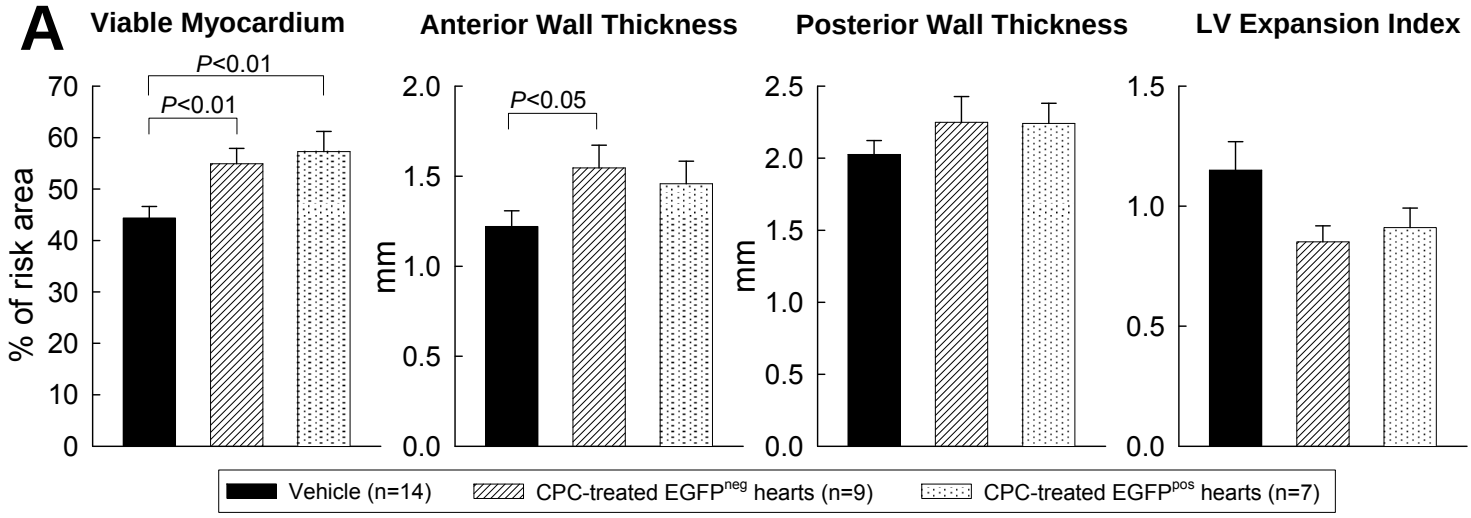

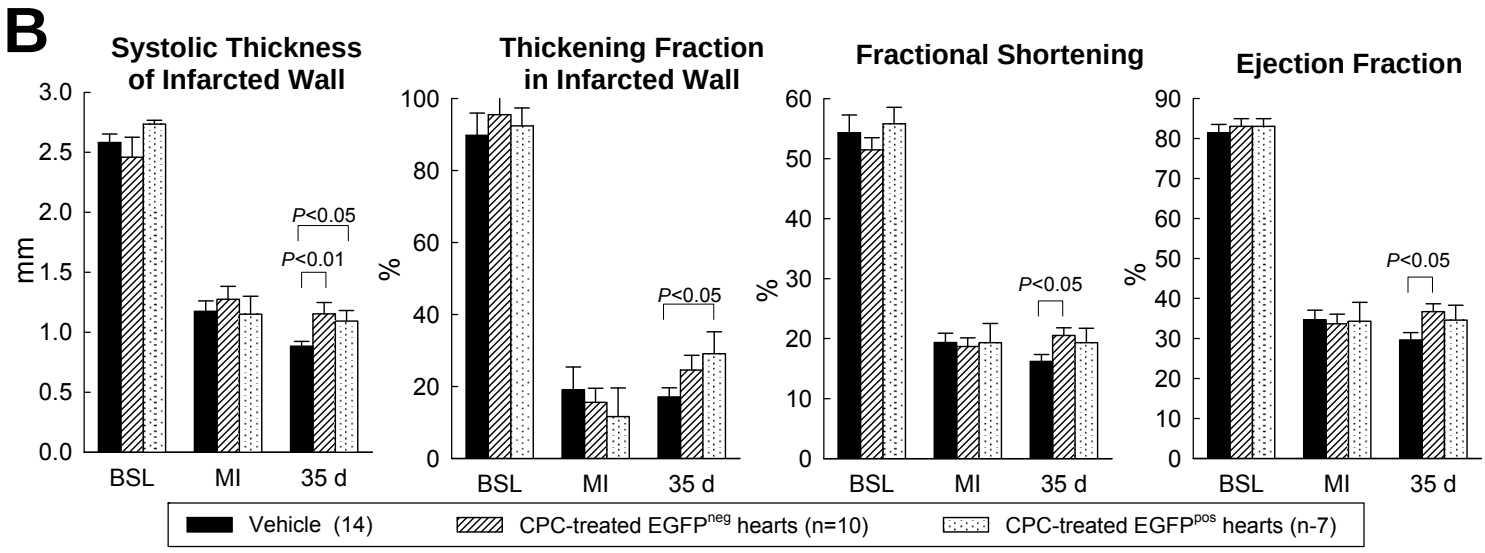

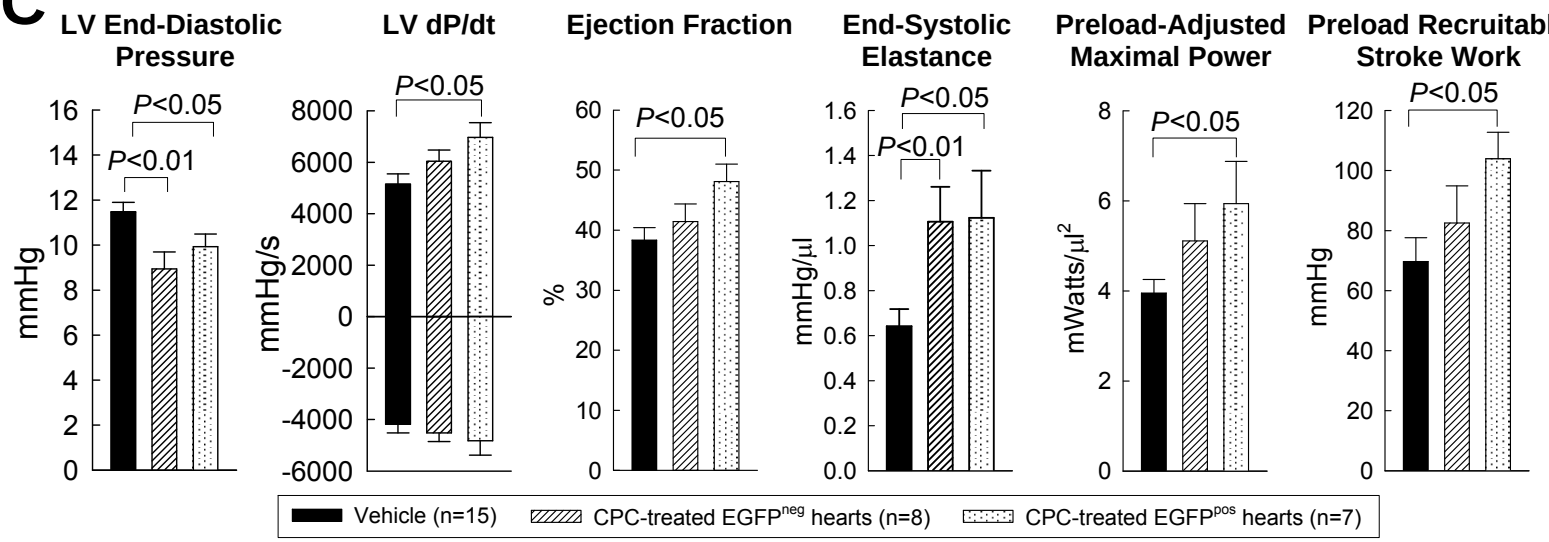

Supplemental Figure 19. **Analysis of LV morphometry and function in the EGFP^{neg} and EGFP^{pos} subsets of CPC-treated rats.** CPC-treated rats were subdivided into two subsets based upon whether they exhibited any EGFP^{pos} cells or no EGFP^{pos} cells. ***(A)*** Morphometric variables (amount of viable myocardium in the risk region, anterior LV wall thickness, posterior LV wall thickness, and LV expansion index). ***(B)*** Echocardiographic variables (systolic thickness of the anterior [infarcted] wall, anterior [infarcted] wall thickening fraction, LV fractional shortening, and LV ejection fraction). ***(C)*** Hemodynamic variables (LV end-diastolic pressure, dP/dt, EF, end-systolic elastance, preload-adjusted maximal power, and preload recruitable stroke work). Data are means ± SEM.

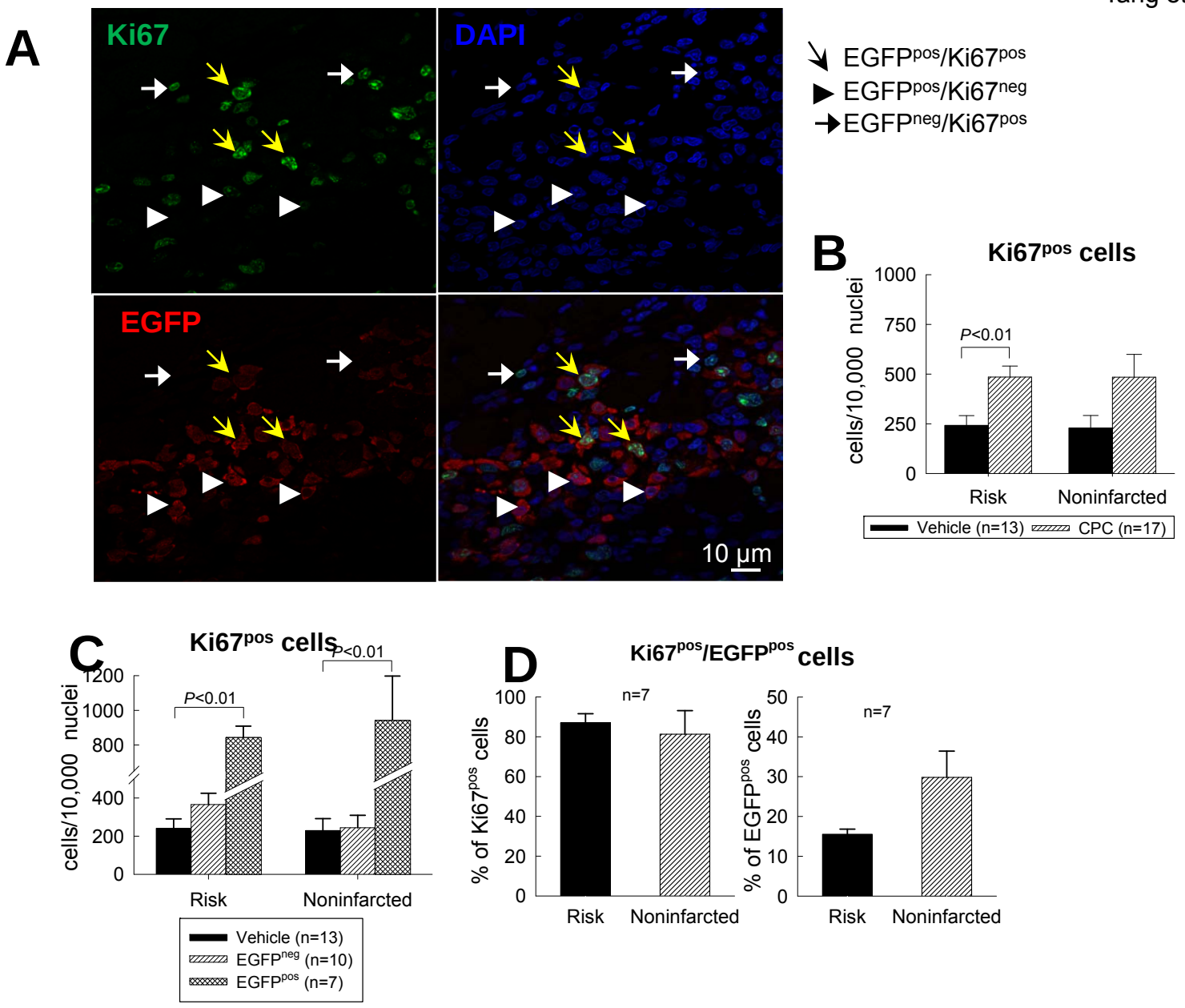

Supplemental Figure 20. **Proliferation of transplanted CPCs.** Proliferation of cells at the time of euthanasia was determined by counting Ki67^{pos} nuclei. Under epifluorescent microscopy, EGFP^{pos}/Ki67^{pos} cells (cells with colocalization of Ki67 [FITC] and EGFP [TRITC]) were counted in the respective fluorescent emission channel. In each heart, one LV slice was selected for quantitation and 6-27 fields were counted (60x magnification; range, 57-445 EGFP^{pos}/Ki67^{pos} cells per slice). (Similar methods were used for the counting of EGFP^{pos}/BrdU^{pos} cells, i.e., cells with colocalization of BrdU [FITC] and EGFP [TRITC]) summarized in Fig. 7; in that case, in each heart, one LV slice was selected for quantitation and 8-28 fields were counted [60x magnification; range, 73-721 EGFP^{pos}/BrdU^{pos} cells per slice]). ***(A)*** Representative confocal microscopic images from a CPC-treated rat showing Ki67 expression in the infarcted region at 35 d after CPC infusion. **Yellow arrows** indicate EGFP^{pos} cells that are Ki67 positive; **white arrowheads** EGFP^{pos} cells that are Ki67negative; and **white arrows** EGFP^{neg} cells that are Ki67 positive. ***(B***, ***C***, and ***D)*** Quantitative analysis of Ki67^{pos} cells in the risk and noninfarcted regions. Panel ***B*** shows the number of Ki67^{pos} cells in vehicle-treated and CPC-treated groups; panel ***C*** shows the same data except that the CPC-treated group is subdivided into the subgroups that did or did not exhibit EGFP^{pos} cells (in the seven hearts with EGFP^{pos} cells, Ki67^{pos} cells were measured in the entire region examined, both in the EGFP^{pos} and in the EGFP^{neg} areas). ***(D)*** Colocalization of Ki67 and EGFP immunoreactivity in the seven CPC-treated hearts that exhibited EGFP^{pos} cells. Data are means ± SEM. A significant increase in Ki67 positivity was noted in the CPC-treated hearts that contained EGFP^{pos} cells, both in the risk and in the noninfarcted regions (***panels B*** and ***C***). As was the case for BrdU^{pos} cells, in the seven CPC-treated rats that exhibited EGFP positivity, the vast preponderance (~85%) of Ki67^{pos} cells were positive for EGFP and, conversely, 16% and 30% of EGFP^{pos} cells were positive for Ki67 in the risk and noninfarcted regions, respectively (***panel D***).

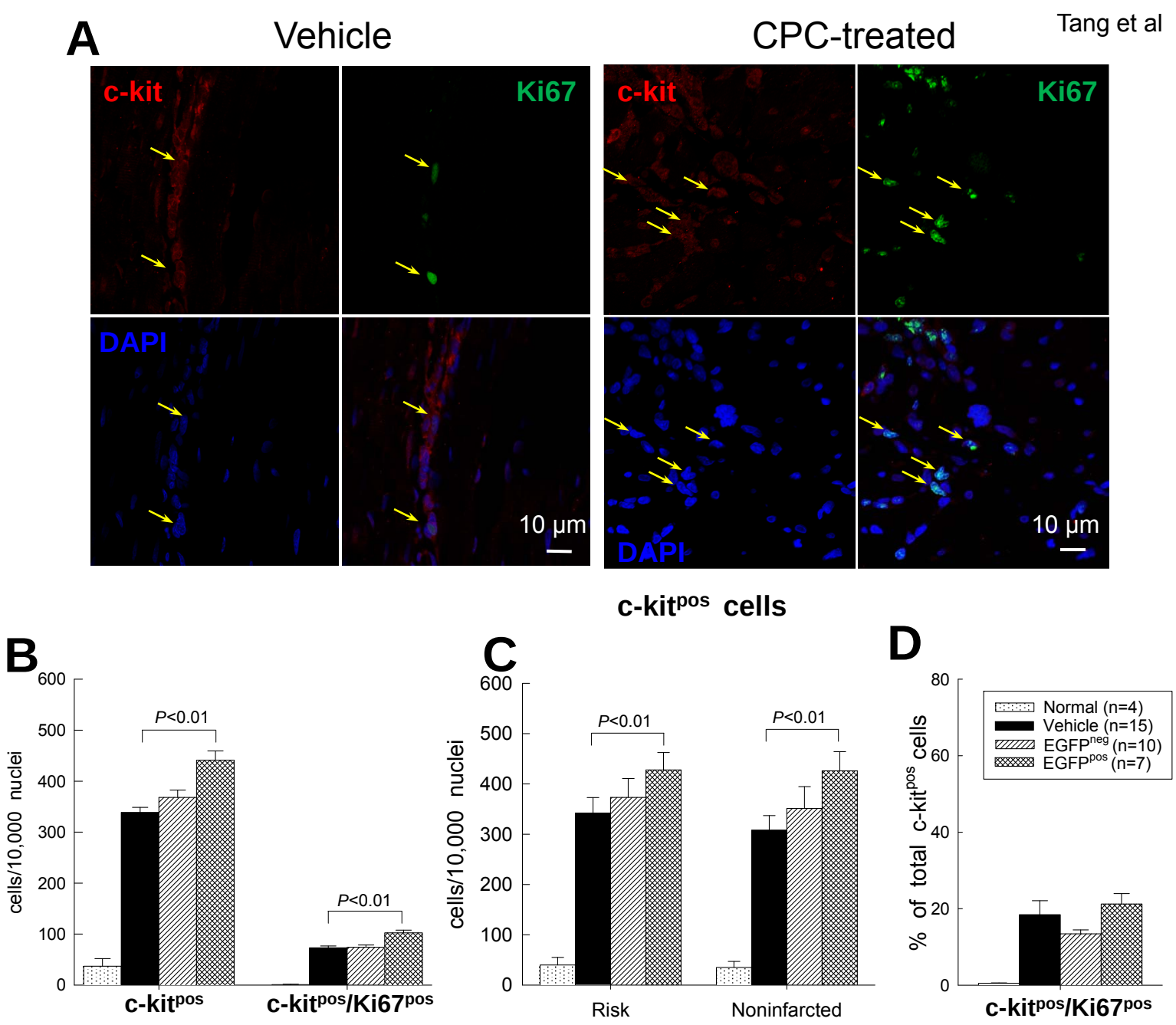

Supplemental Figure 21. Effect of CPC transplantation on c-kit^{pos} cells. Under epifluorescent microscopy, c-kit^{pos}/Ki67^{pos} cells (cells with colocalization of c-kit [TRITC] and Ki67 [FITC]) were counted in the respective fluorescent emission channel. In each heart, one LV slice was selected for quantitation and 24 fields were counted (60x magnification; range, 18-124 c-kit^{pos}/Ki67^{pos} cells per slice. (Similar methods were used for counting c-kit^{pos}/BrdU^{pos} cells. i.e., cells with colocalization of c-kit [TRITC] and BrdU [FITC] summarized in Fig. 8; in that case, one LV slice was selected for quantitation and 24 fields were counted [60x magnification; range, 68-208 c-kit^{pos}/BrdU^{pos} cells per slice]). ***(A)*** Representative confocal microscopic images from a vehicle-treated and a CPC-treated rat showing c-kit^{pos} cells (red) and Ki67^{pos} cells (green) in the risk region. **Yellow arrows** indicate cells that co-express c-kit and Ki67. ***(B)*** Quantitative analysis of c-kit^{pos} cells and double positive (c-kit^{pos}/Ki67^{pos}) cells in normal, vehicle-treated, and CPC-treated hearts (the last group is subdivided into two subgroups, that with EGFP^{pos} cells [EGFP^{pos}] and that without EGFP^{pos} cells [EGFP^{neg}]). ***(C)*** Quantitative analysis of c-kit^{pos} cells in the risk and noninfarcted regions in normal, vehicle-treated, and CPC-treated hearts [as in (B), the last group is subdivided into EGFP^{pos} and EGFP^{neg} subgroups]. ***(D)*** Quantitative analysis of double positive (c-kit^{pos}/Ki67^{pos}) cells expressed as a percent of all c-kit^{pos} cells. Data are means ± SEM.

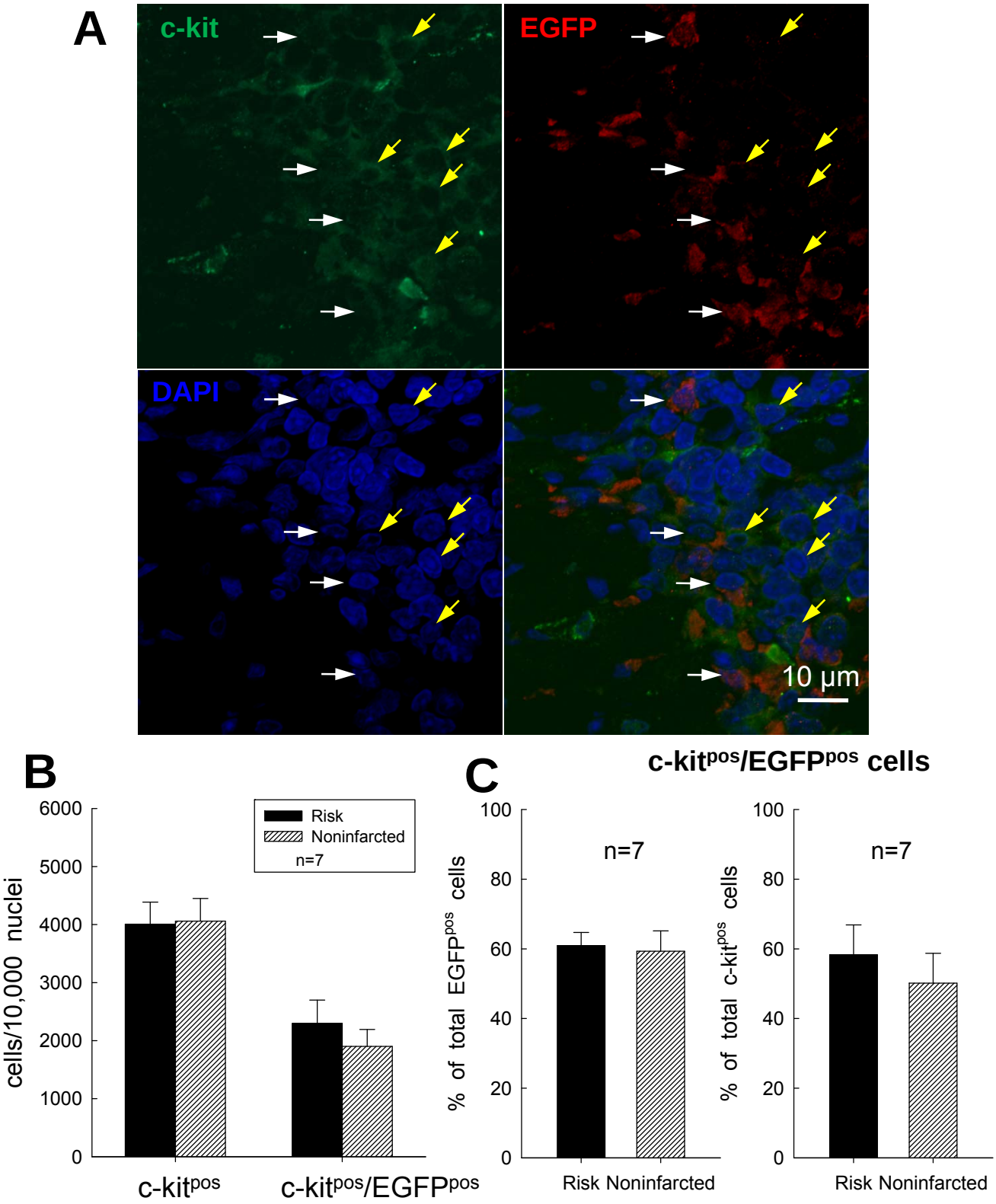

Supplemental Figure 22. Effect of CPC transplantation on c-kit^{pos} cells. To determine the effect of CPC transplantation on endogenous CPCs (c-kit^{pos} cells), the coexpression of c-kit and EGFP was determined in the seven CPC-treated hearts that contained EGFP^{pos} cells. ***(A)*** Representative confocal microscopic images from a CPC-treated rat showing c-kit^{pos} cells (green) and EGFP^{pos} cells (red) in the border zone. **White arrows** indicate c-kit^{pos} cells that are EGFP^{pos} (i.e., exogenous CPCs or their progeny), whereas **yellow arrows** indicate c-kit^{pos} cells that do not express EGFP and thus likely represent endogenous CPCs. ***(B)*** Quantitative analysis of c-kit^{pos} cells and double positive (c-kit^{pos}/EGFP^{pos}) cells in the risk and noninfarcted regions. ***(C)*** Quantitative analysis of double positive (c-kit^{pos}/EGFP^{pos}) cells in the risk and noninfarcted regions expressed as a percent of all EGFP^{pos} cells (left side) and all c-kit^{pos} cells (right side). Data are means ± SEM. The finding that, in the seven CPC-treated hearts that had EGFP^{pos} cells, ~half of the c-kit^{pos} cells were EGFP^{neg} further supports the conclusion that endogenous CPCs were activated by exogenous CPCs.

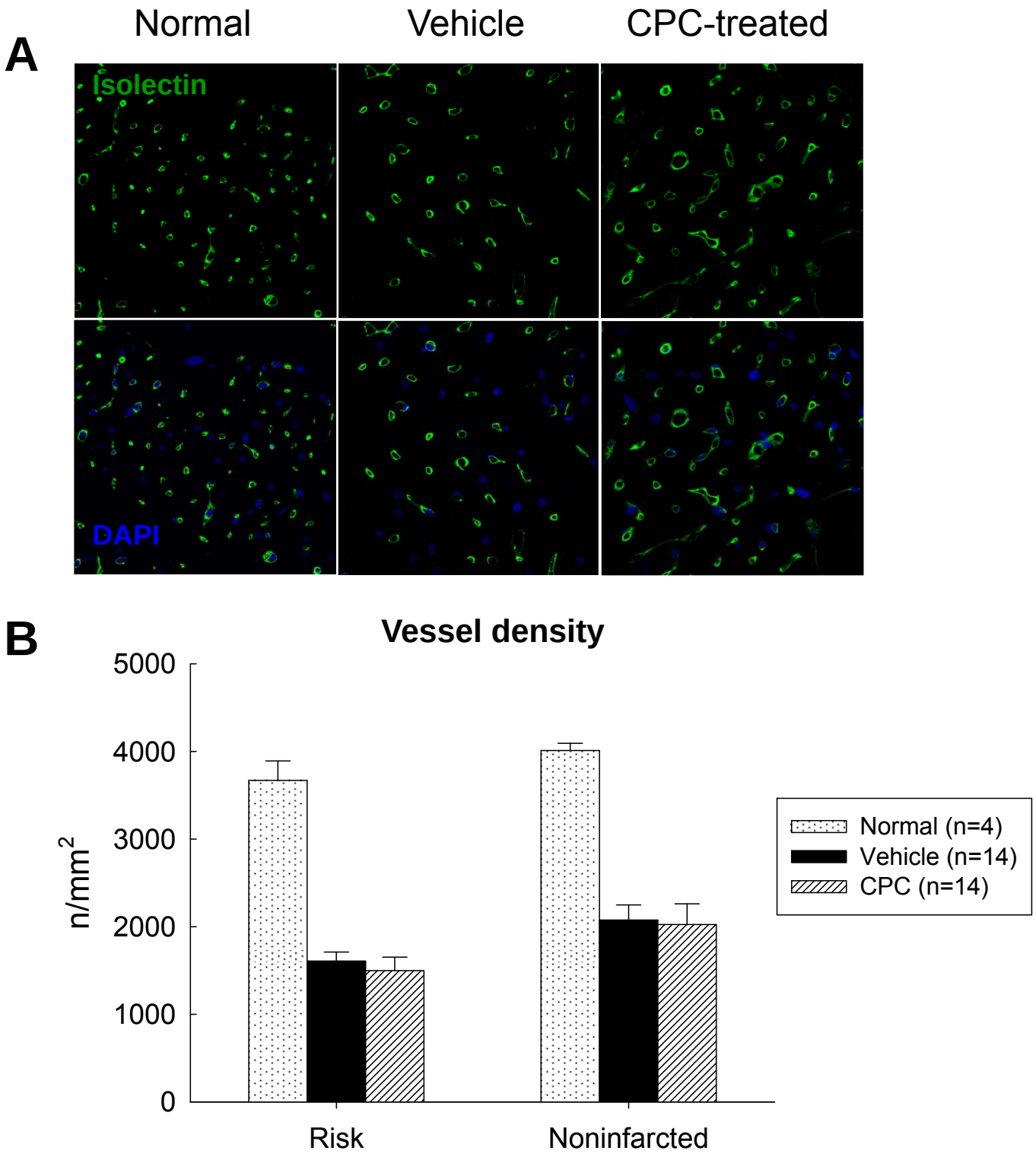

Supplemental Figure 23. **Analysis of vessel density by isolectin staining.** Vessel density was determined in vehicle- and CPC-treated hearts by staining vascular endothelium with FITC-conjugated isolectin B4. ***(A)*** Representative confocal microscopic images from a normal, a vehicle-treated, and a CPC-treated rat (in the latter two, the images were taken from the border zone) showing FITC-conjugated isolectin B4-stained vessels counterstained with DAPI. ***(B)*** Vessel density was determined in normal, vehicle-treated, and CPC-treated groups by counting vessels stained with isolectin B4 and normalized to area. There were no differences in vessel density between vehicle- and CPC-treated hearts at 35 days after treatment Data are means ± SEM.

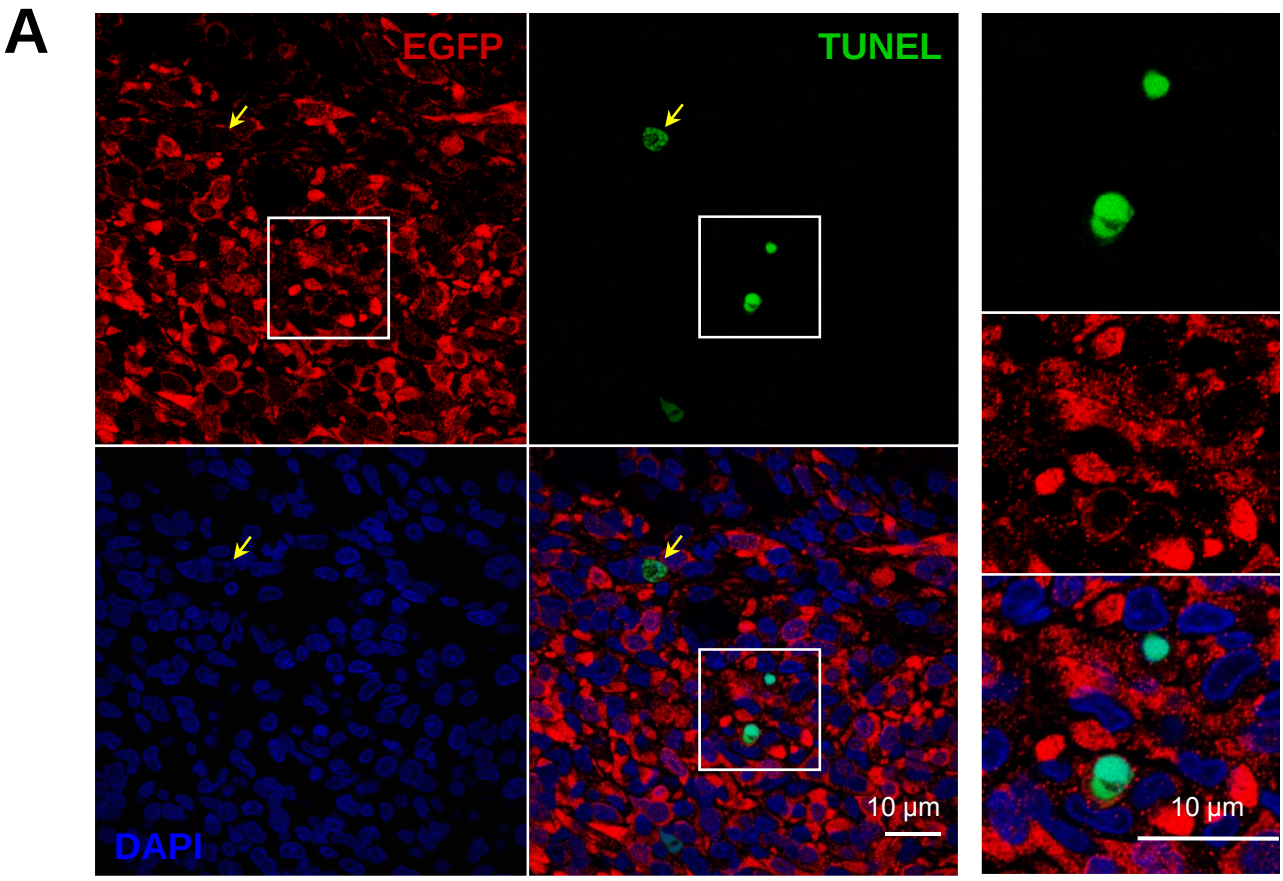

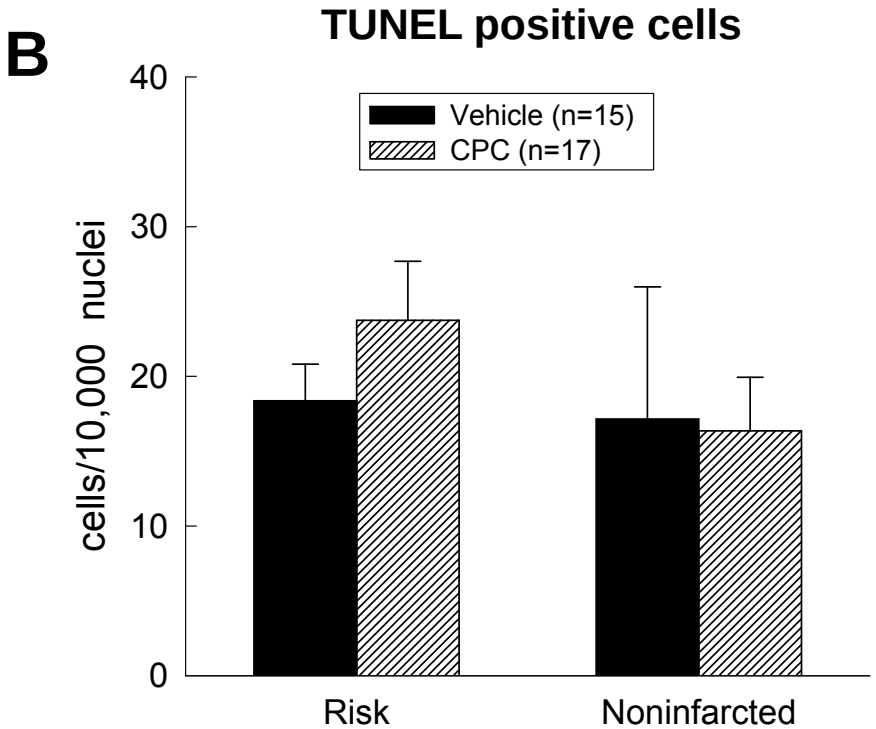

Supplemental Figure 24. **Analysis of apoptosis by TUNEL staining.** Cells undergoing apoptotic death in vehicle- and CPC-treated hearts were identifed by TUNEL staining. ***(A)*** Representative confocal microscopic images in the border zone of a CPC-treated rat showing TUNEL positive nuclei (green), EGFP staining (red), DAPI staining (blue), and a merge of EGFP, TUNEL, and DAPI staining. The white box (magnified in the three panels on the right) contains two $EGFP^{pos}$ cells that are also TUNEL positive. The **yellow arrow** indicates a cell that is TUNEL positive but $EGFP^{neg}$.***(B)*** Quantitative analysis of TUNEL positive nuclei in the risk and noninfarcted region in the vehicle- and CPC-treated groups. There were no differences in TUNEL positive nuclei between vehicle- and CPC-treated hearts at 35 days after treatment. Data are means ± SEM.

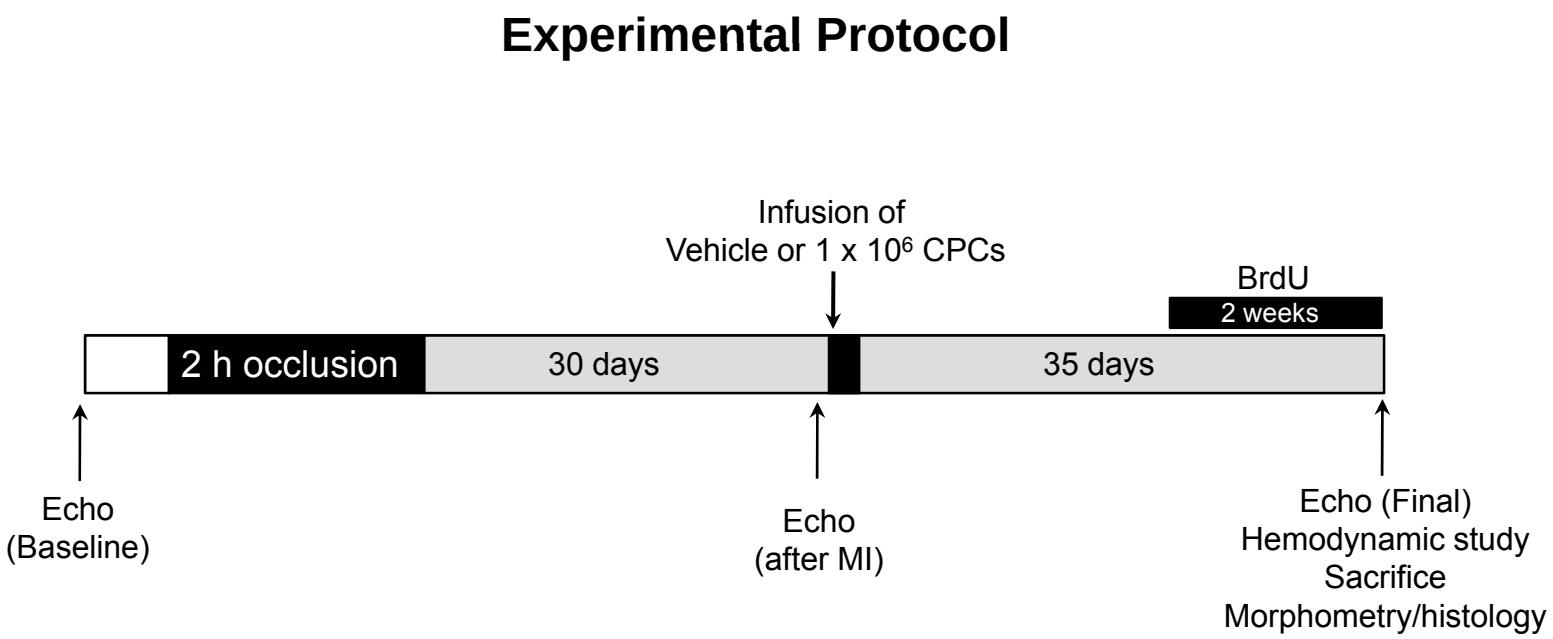

Supplemental Figure 25. Experimental protocol. Echo, echocardiographic examination.

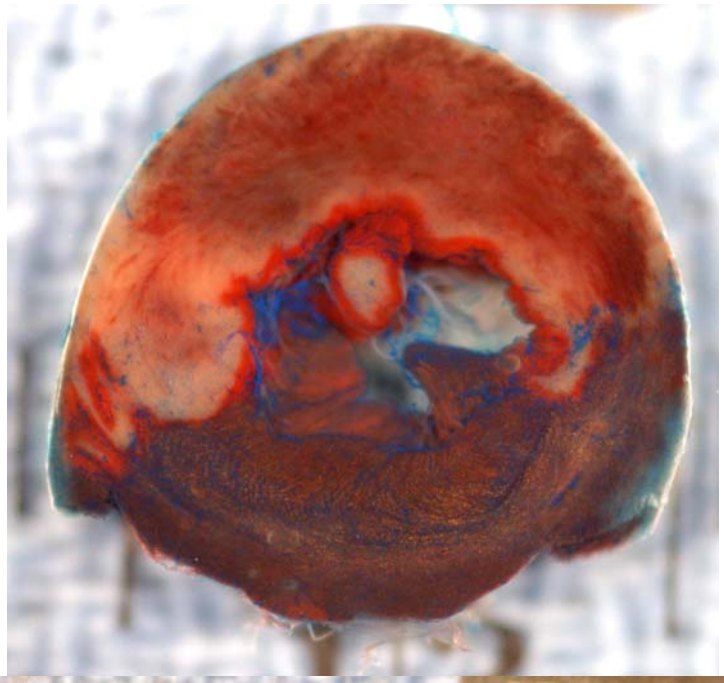

Risk region:
54.8% of LV

Infarct size:
91.0% of risk region
49.9% of LV

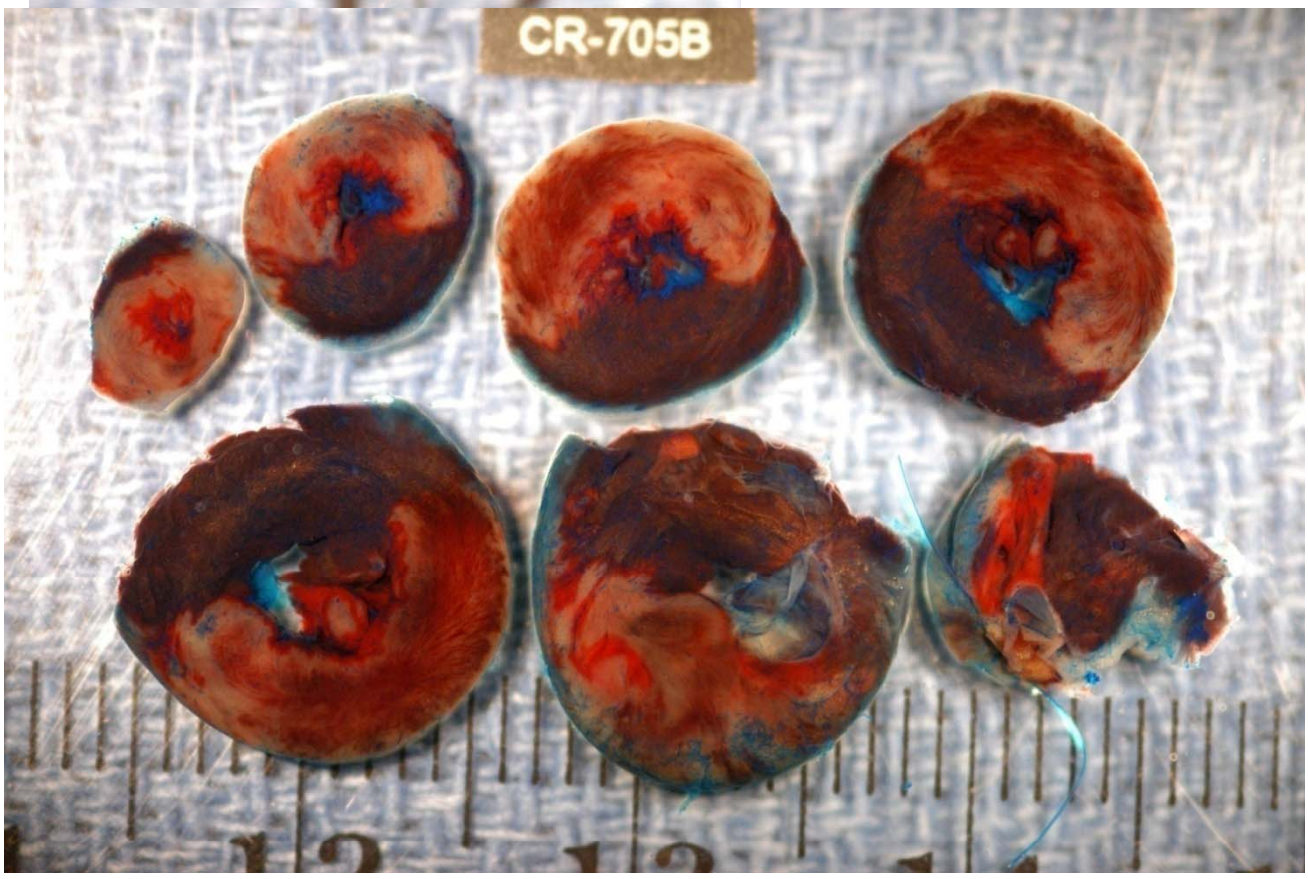

<u>Supplemental Figure 26</u>. Myocardial infarct size after a 2-h coronary occlusion and 24 h of reperfusion. The rat was subjected to coronary occlusion/reperfusion as described in Methods. The heart was perfused with a 1% solution of triphenyl tetrazolium chloride (to delineate myocardial infarction) and then with a 5 % solution of phthalo blue dye (to delineate the occluded-reperfused coronary vascular bed) after the coronary artery was tied at the site of the previous occlusion. As a result of this procedure, the nonischemic region was stained dark blue whereas the portion of the LV supplied by the previously occluded coronary artery (risk region) was identified by the absence of blue dye. The LV slices were photographed and planimetry was performed using the NIH ImageJ software. Note the massive transmural infarct with obvious hemorrhage.